POLITECNICO DI MILANO

School of Civil Environmental and Land Planning Engineering

Master of Science degree in Environmental and Land Planning Engineering

UPPSALA
UNIVERSITET

Tidal Effect Compensation System for Wave Energy Converters

Supervisor: Mats LEIJON

Co-supervisor: Giuseppe PASSONI

Valeria CASTELLUCCI

Matr. 735148

Academic Year 2010/2011

To the most precious gift,

my family.

Abstract

Recent studies show that there is a correlation between water level and energy absorption values for wave energy converters: the absorption decreases when the water levels deviate from average. The effect for the studied WEC version is evident for deviations greater then 25 cm, approximately. The real problem appears during tides when the water level changes significantly. Tides can compromise the proper functioning of the generator since the wire, which connects the buoy to the energy converter, loses tension during a low tide and hinders the full movement of the translator into the stator during high tides.

This thesis presents a first attempt to solve this problem by designing and realizing a small-scale model of a point absorber equipped with a device that is able to adjust the length of the rope connected to the generator. The adjustment is achieved through a screw that moves upwards in presence of low tides and downwards in presence of high tides. The device is sized to one-tenth of the full-scale model, while the small-scaled point absorber is dimensioned based on buoyancy's analysis and CAD simulations. Calculations of buoyancy show that the sensitive components will not be immersed during normal operation, while the CAD simulations confirm a sufficient mechanical strength of the model.

A stepper motion system is used to drive the motor which enables the screw to move. The motor is able to produce a high torque, capable of overcoming the Archimedes' force for the model. The device is additionally demonstrated to be self-locking. A LabVIEW program is written to automate the control and help the user to interface with the motion system. Tides are represented as sine functions and the frequency with which to monitor the water level can be chosen as well as the rotational speed of the motor. Once these parameters are set, the motor adjusts the position of the screw automatically.

Numerical results as well as experimental tests carried out in the tank of the department's workshop show that the solution adopted to minimize the tidal effect on the power generation is working, and shows potential for further development.

Keywords: sea wave energy; wave energy converter; real time control; tidal waves.

Sommario

L'obiettivo del Progetto Lysekil, iniziato nel 2002 presso l'università di Uppsala, è quello di verificare un nuovo metodo di conversione di energia dalle onde dell'oceano. I convertitori di energia sono collocati nella località di Lysekil, sulla costa occidentale della Svezia, e producono elettricità sfuttando la variazione di campo magnetico nel generatore posto sul fondo del mare. Una boa in superficie si muove inseguendo le oscillazioni delle onde e guidando il movimento di un pistone a cui è collegato tramite una fune. Il pistone circondato da magneti si muove, quindi, verticalmente all'interno di uno statore, inducendo corrente negli avvolgimenti dello statore stesso.

L'assorbimento di energia dipende dal livello medio dell'acqua che varia in presenza di alte e basse maree. Studi recenti mostrano che l'assorbimento diminuisce quando la variazione di livello supera i 25 cm. Per questa ragione, le maree possono compromettere il corretto funzionamento dei convertitori di energia.

Una possibile soluzione a questo problema è ampiamente discussa in questa tesi che descrive la progettazione e la realizzazione di un modello in scala di un nuovo tipo di generatore: la boa è equipaggiata con un dispositivo che modifica la lunghezza della fune durante le maree. In particolare, una vite a cui la fune è legata si muove verso il basso durante l'alta marea e verso l'alto durante la bassa marea. Simulazioni CAD e analisi di galleggiabilità hanno permesso di giungere a un corretto dimensionamento dell'elemento flottante, considerando che per il dispositivo di regolazione è stato scelto un rapporto 1 a 10 rispetto al modello in scala reale.

Il movimento della vite è guidato da un motore, il quale viene automaticamente controllato da un programma LabVIEW una volta impostata la frequenza di controllo e la velocità a cui il motore deve operare.

Secondo le analisi da galleggiabilità le parti sensibili non vengono immerse durante le normali operazioni, mentre le simulazioni in SolidWorks mostrano che il modello è sufficientemente robusto dal punto di vista meccanico. Analisi numeriche dimostrano che il dispositivo è auto-bloccante, cioè la vite non è soggetta a svitamenti, ma mantiene la posizione desiderata anche quando la fune è sottoposta ad elevate tensioni.

Il modello in scala è stato testato in vasca al fine di valutare il corretto funzionamento del dispositivo. Le onde sono state riprodotte grazie ad un generatore d'onda montato all'interno della vasca, mentre le maree sono state simulate cambiando il livello medio dell'acqua.

Risultati numerici e analisi sperimentali dimostrano che la soluzione proposta in questa tesi per la minimizzazione dell'effetto di marea sulla produzione di energia elettrica dalle onde degli oceani è fattibile e si presta a futuri studi.

Contents

Nomenclature and abbreviations **xvii**

1 Introduction **1**

1.1 Renewable energy 1

1.2 Wave energy 3

1.2.1 Goals 4

1.2.2 The concept 5

1.3 The Lysekil Project 6

1.3.1 Strategy 7

1.3.2 History 8

1.3.3 Environmental impact 10

2 Theory **13**

2.1 Linear theory of ocean waves 13

2.2 Theory of tides 18

2.2.1 Lunar and Solar tides 18

2.2.2 Acting forces 19

2.2.3 Configuration of free surface 21

2.2.4 Water level measurement 22

2.2.5 Tides around the world 24

2.3 3D CAD Design with SolidWorks 26

2.4 Control System with LabVIEW^{TM} 28

3 Experimental work **31**

3.1 Small scale model 32

3.1.1 Buoyancy 37
3.1.2 Friction and torque 39
3.2 Simulations 45
3.3 Motion Control 49
3.3.1 Stepper Motion System 50
3.3.2 Front Panel 52
3.3.3 Block Diagram 54
3.4 Laboratory experiments 59
3.4.1 Simulation of tide 59
3.4.2 Program in LabVIEW 60
3.4.3 Small scale generator 62

4 Results and discussion **63**

5 Conclusion **75**

6 Future work **79**

Acknowledgments **81**

References **83**

List of Tables

3.1 Buoyancy of the small-scale model. 38
3.2 The variation of F_{wire}. 38
3.3 Data referring to screw and nut. 41
3.4 Results for the system screw-nut. 41
3.5 Results for the system screw-nut. 42
3.6 Data referring to worm wheel and worm. 42
3.7 Results for the worm. 43
3.8 Weight of the device's components. 45
3.9 Pump's specifications. 60

4.1 Torque necessary to hold the buoy under the water level. 65
4.2 Efficiency of the inclined planes. 67
4.3 Values of both $\tan\theta_{screw}$ and $\tan\theta_{worm}$. 68
4.4 Produced voltage, numerical results. 73
4.5 Produced voltage, percentage. 73

5.1 Torque for different friction coefficients. 76
5.2 Torque for the submerged buoy. 76
5.3 Maximum displacement and stress for both bearing and housing. . . 76

List of Figures

1.1 Degree of utilization. 2
1.2 Utilization for different source of energy. 2
1.3 Converter. 5
1.4 Lysekil's factory. 6
1.5 Biological life around the WEC. 11

2.1 Water particle orbits in deep water. 16
2.2 Water particle orbits in shallow water. 16
2.3 Shallow water waves. 18
2.4 Spring and Neap Tides. 19
2.5 Forces acting on the unit mass of water on Earth's surface. 20
2.6 The configuration of the water surface. 22
2.7 Tide gauge. 23
2.8 Global map of tidal waves. 24
2.9 Skagerrak and Kattegat seas. 25
2.10 Monthly and annual water level averages in the port of Ålesund. . . 25
2.11 Predicted tide table for Ålesund. 26
2.12 Lunar tide in the Mediterranean. 27
2.13 Logo of SolidWorks Premium 2010. 27
2.14 LabVIEW icon, by National Instruments. 28
2.15 Example of a LabVIEW program. 30

3.1 Viable solution to minimize the tidal effect. 31
3.2 Small-scale model drawn with SolidWorks. 33
3.3 TR10x3 screw. 33

3.4 The device and its section. 34
3.5 Virtual and real device. 34
3.6 The motor. 35
3.7 The U-seal. 35
3.8 Polystyrene floater. 36
3.9 Epoxy resin. 37
3.10 Immersed volume of the CAD model. 39
3.11 Self-locking device. 40
3.12 Schematization of the worm wheel (cog) and the worm. 43
3.13 Force and torque. 43
3.14 Overview of the nut and the screw. 44
3.15 Bearing's displacement plot. 46
3.16 Bearing's stress plot. 46
3.17 Top view of the bouy. 47
3.18 Housing's displacement plot. 48
3.19 Housing's stress plot. 48
3.20 Components of a Motion Control System. 49
3.21 Stepper motor. 51
3.22 Hardware components of the Stepper Motion Control System. 51
3.23 Front panel of the LabVIEW program. 53
3.24 Block diagram of the LabVIEW program. 55
3.25 Sub-VI ENABLE. 56
3.26 Sub-VI ENABLE 1. 56
3.27 Sub-VI UP or DOWN. 57
3.28 Sub VI WAVE HEIGHT. 57
3.29 Sub-VI LAST VALUE. 57
3.30 Simple One-Axis Move VI. 58
3.31 Sub-VIs CONV and SCREW. 58
3.32 The tank. 59
3.33 Worldcraft Pump. 60
3.34 Front panel of the second LabVIEW program. 61

3.35 The small scale generator. 62

4.1 Oscilloscope. 64
4.2 The motor is able to hold the buoy under the water. 65
4.3 Theoretical and experimental buoyancy curves. 66
4.4 Dynamometer. 67
4.5 The model is tested in presence of waves. 68
4.6 MT Profil tank contents gauge. 70
4.7 Frequency of the control. 71
4.8 Produced voltage, experimental results. 72

5.1 How the real buoy can look like. 77

Nomenclature and abbreviations

Chapter 1

U	%	Utilization
W	Wh	Average annual energy
P	W	rated power

Chapter 2

$\overline{v}$	m/s	Velocity vector
ϕ	m^2/s	Velocity potential
h	m	Water depth
η	m	Free surface elevation
g	m/s^2	Acceleration of gravity
C	m/s	Celerity
L	m	Wavelength
T	s	Period
k	1/m	Wave number
ω	rad/s	Angular frequency
a	m	Wave amplitude
f_c	m/s^2	Centrifugal force
f_a	m/s^2	Moon's attraction
f_g	m/s^2	Earth's attraction
M_m	kg	Moon's mass
M_e	kg	Earth's mass
l_e	m	Distance between Earth and the axis of revolution Earth-Moon
l_m	m	Distance between Moon and the axis of revolution Earth-Moon
l	m	Distance between Earth and Moon
G	Nm^2/kg^2	Gravitational constant
r_e	m	Earth's radius
s	m	Distance between the unit mass of water and the Moon
F_r	m/s^2	Radial force
F_t	m/s^2	Tangential force
α	rad	Earth's central angle
β	rad	Moon's central angle

Chapter 3

F_{buoy}	N	Buoy 's weight force
F_{arch}	N	Archimedes' force
W_{buoy}	kg	Buoy's weight
ρ_w	kg/m^3	Water density
ρ_{buoy}	kg/m^3	Buoy's average density
V_{buoy}	mm^3	Buoy's volume
$\%V_i$	%	Percentage of immersed volume
F_{res}	N	Difference between F_{buoy} and F_{arch}
I_{buoy}	cm	Immersion
F_{wire}	N	Force in the wire
$F_{friction}$	N	Friction force
μ	-	Friction coefficient
F_{normal}	N	Normal force
θ	rad	Inclined plane angle
D_{screw}	m	Screw's diameter
m_{ps}	kg	Piston-screw's mass
F_{drag}	N	Drag force
P_{screw}	m	Pitch of the screw
M	Nm	Torque necessary to move the screw
F_k	N	Force operating between worm wheel and worm
r_k	m	Worm wheel's radius
D_s	m	Worm wheel's diameter
P_{worm}	m	Pitch of the worm
M_s	Nm	Torque the engine has to deliver
μ	-	Efficiency of the inclined plane
μ_{screw}	-	Efficiency referred to the screw
μ_{worm}	-	Efficiency referred to the worm
ϕ	rad	Friction angle

Chapter 4

P	W	Instantaneous active power
V_{RMS}	V	Voltage
I_{RMS}	A	Current
θ	rad	Phase difference between V and I
M_s	Nm	Torque delivered by the motor
v	m/s	Motor's speed

Abbreviations

AC	Alternating Current
CAD	Computer-Aided Drafting
CFE	Swedish Centre for Renewable Electric Energy Conversion
DC	Direct Current
FEA	Finite Element Analysis
GRP	Glass-reinforced plastic
LRS	Lysekil Research Site
NBR	Nitrile butadiene rubber
NI	National Instruments
UMI	Universal Motion Interface
VDC	Volts of direct current
VI	Virtual instrument
WEC	Wave Energy Converter

Chapter 1

Introduction

1.1 Renewable energy

The ever increasing need for energy in the world puts a focus on renewable energy technologies. In order to know in which field it is better to invest money to have a good cost-benefit ratio, it is necessary to develop a method to evaluate the technical and economical competitiveness of the source. A first indication of the potential of a renewable source is the Degree of Utilization:

$$U = \frac{W}{P * 8760} * 100[\%]$$

where

- U is the degree of utilization;
- W is the average annual energy delivered to the electric grid;
- P is the rated power of the power plant;
- 8760 is the number of hours in a year.

Figure 1.1 gives an idea about what these variables represent.

Recent studies [1] show that wave power, together with marine current power, is a way of generating electricity with higher degrees of utilization then both solar PV and wind power, see Figure 1.2.

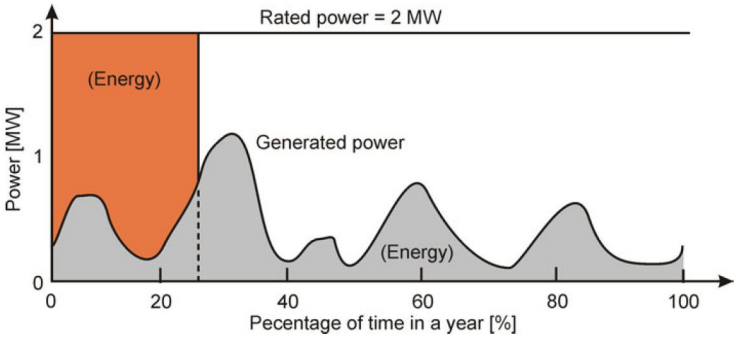

Figure 1.1: The gray area represents the energy generated at varying power during one year. If this energy was generated during part of the year at rated power, the utilization would be the orange area.

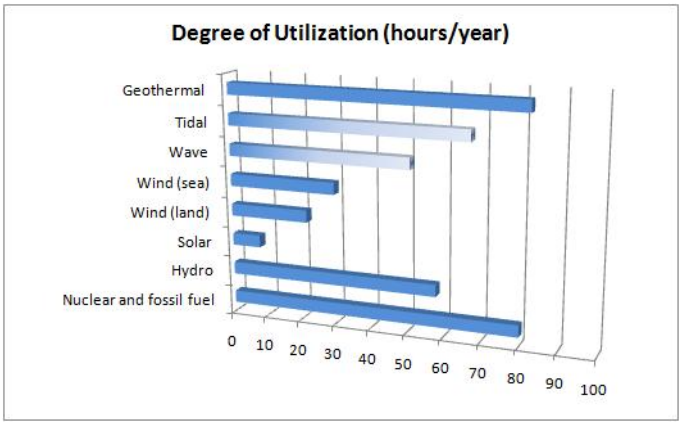

Figure 1.2: Degrees of utilization for different source of energy. Wave power has got a degree of utilization of 35 to 50% depending on difference between the Baltic Sea and the west coast of Sweden. However, in bigger seas or oceans it can go up to 70%.

Depending on location, wave energy is expected to have a potential for utilization levels between 35% and 70% [2]. The International Energy Agency has estimated that wave energy could eventually meet over 10% of the world's current electricity demand [3]. Calculations of the total wave energy flux in the world yeild average values between 1 and 10 TW.

1.2 Wave energy

Ocean waves are caused by the wind as it blows across the open expanse of water, the gravitational pull from the sun and moon, and changes in atmospheric pressure, earthquakes, etc. Waves created by the wind are the most common ones and the most relevant for wave energy technology. They absorb the energy from winds blowing over large areas of ocean surface. Waves, in comparison with winds, are more predictable and more uniformly distributed in time. Even if the wind ceases, waves will keep rolling in for some time. Wave energy is also an irregular oscillating low-frequency energy source. Waves are a powerful source of energy, but they are difficult to harness and convert into electricity in large quantities. The major difficulty is to build systems economically viable and capable to survive harsh weathers and storms, indeed there is a risk of ending up with systems that are too fragile to endure the large mechanical stress as a result of large peak forces. Some other reasons why the scientific community is still struggling with this resource are the difficulty to reach for work and maintenance because of the challenging conditions that working in the ocean involves, the corrosion of metal objects, the fatigue loads the converter must be dimensioned for, the energy price which must be competitive in the electric market, the environmental impact on the landscape and marine life.

It is difficult to evaluate the true amount of power available from waves. However, oceans carry enough energy to merit further study. The existing projects on this topic can be classified regarding the kind of converter used to generate electricity:

- wave activated bodies, where the motion of the waves is directly transfered to the wave energy converter (WEC),

- overtopping devices, which let water run up a slope into a reservoir, from where

the potential energy is converted using a low-head turbine,

- oscillating water columns, which use a fluctuating air pressure above the ocean surface to drive a turbine.

Among the most famous projects Pelamis [4], Wave Dragon [5] and Limpet OWC [6] excel for each typology respectively . The Lysekil Project, developed at Uppsala University, is based on a technology classifiable as a wave activated body, but with a clarification: it is also a so called point absorber, because the width of the WEC is small in comparison to the wave length.

1.2.1 Goals

The wave power project developed in Uppsala University has many goals:

1. to verify that the basic technology for a new wave power concept is successful;

2. to evaluate alternative solutions, e.g. testing several buoys varying in material, size and design;

3. to develop generators adapted to the motion of ocean waves, and a connected electrical system to optimize energy absorption;

4. to gain knowledge of the effects of this new type of wave power plant on the local environment.

Today, the project has permission to install a maximum of 10 generators, each one with an installed capacity of 10-25 kW. The installation of 10 units, corresponding to the production of 100-250 kW, will produce about 300,000-750,000 kWh per year, the equivalent of the yearly consumption of about 15-40 households which use electrical heating, or 60-150 households if the heating is not included. This scenario is suitable for Swedish waters, which have relatively small waves. For bigger waves (Norway or Scotland) bigger units with powers of 100 kW or higher are more advantageous.

1.2.2 The concept

The wave power concept differs in many ways from earlier attempts: Uppsala University developed a totally new solution able to contribute to the energy supply with a robust and economically competitive system. The concept is based on a generator situated on the seabed and connected through a rope to a buoy on the surface, see Figure 1.3.

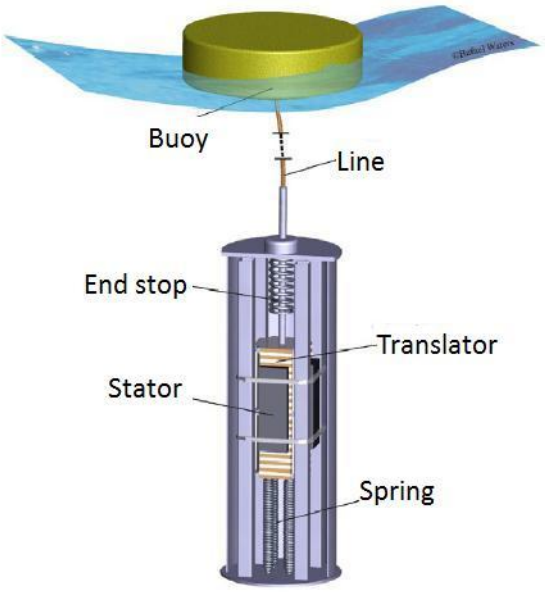

Figure 1.3: Sketch of the converter by Rafael Waters.

The translator moves up and down in the stator, driven directly via the rope by the buoy motion on the surface. The piston is equipped with very strong neodymium-iron-boron (Nd-Fe-B) magnets and induces currents in the stator's windings. In addition, the piston is connected to a spring system, which gives the generator additional power also when the buoy is moving down in a trough. A generator placed on the seabed is protected from harsh weather. Moreover, if a buoy should break it is a cheap component to replace. Another advantage of the technology is that it is modular. Wave power plants can consist of a suitable number of units and, as the demand grows, more units can be added. Furthermore, if a unit is out of service, the installation is not compromised. On the other hand, the WEC technology has some remaining challenges. Recent studies show that there is a correlation

between water level and energy absorption values: the absorption decreases when the water levels deviate from average. The effect is noticeable for the whole range of water level values, but is not very prominent for deviations smaller then 25 cm [8]. The real problem appears concomitantly with tides, i.e. when the water level changes significantly. Tides can compromise the proper functioning of the generator, in fact the length of the wire, which connects the buoy to the energy converter, loses tension during a low tide and hinders the full movement of the translator into the stator during high tides. The goal of the thesis will be to suggest a solution to this issue.

1.3 The Lysekil Project

The work presented in this thesis is closely linked to the Lysekil Project, that takes its name from the wave energy research site, developed since 2004 by Uppsala University, related to the Swedish Center for Renewable Electric Energy Conversion (CFE). The experimental work has taken place both at the Ångström Laboratory in Uppsala and at Lysekil.

Figure 1.4: Point absorbers in the Lysekil's factory.

This research site is located on the Swedish west coast and here both technical and biological research will be carried out until 2014. The choice of Lysekil as the location for a research park is due to the good wave climate, the easy accessibility both by sea and land, the closeness to the main grid and the proximity to Uppsala

University's Biological Station and Kristineberg Marin Research Station. The depth at the site is 25 m and the seabed is made of one meter of sandy silt. On the research site, some generators and one marine substation have been deployed, moreover several dummy buoys are available for biological research. The WECs are connected to a measuring station on the nearby island of Härmanö. There is also a *wave rider*, a wave measuring buoy to monitor the sea state, and an *observation tower* to study the buoys' motion. The mean energy flux at the Lysekil research site, based on a study of eight years of satellite data, is 2.6 ± 0.3 kW/m [7]. The wave energy is primarily available in combinations of significant wave heights of about $1-3$ m and wave periods of about $4-7$ s. Concomitantly with this sea state, the 10-25% of the total energy from waves was converted to electricity in early experiments.

1.3.1 Strategy

The strategy adopted in the Lysekil wave energy project was based on few guiding principles:

- simple mechanics, in order to minimize the need for maintenance,
- electrical loads rather then mechanical loads, preferring high electrical loads rather then high mechanical loads,
- keep expensive and sensitive parts away from the surface, where the impact from loads, corrosion and marine life is greater,
- holistic perspective, where decisions are made keeping in mind the entire chain from capturing to supplying energy of good quality to the electric grid [8].

The point absorber follows the motion of the waves, producing electricity thanks to the motion of the translator along the stator. The generated electricity is converted from its original form to the suitable frequency and amplitude through power electronic components: the generated alternating voltage is rectified and then inverted back to AC of the desired frequency. In order to avoid high transmission losses during the electricity transfer to the shore, it's possible to make this conversion near the WECs, in one or more substations connected to the generators.

1.3.2 History

In this section, the key events of the project are itemized.

2002/2004

- During the spring of 2002 the Lysekil Project got started.
- Some studies about the condition of the seabed were made during the summer of 2003.
- The first linear generator for laboratory experiments was completed at the end of the same year.
- In April of 2004 a wave measuring buy was settled in Lysekil Research Site (LRS).
- Some samples were taken from the seabed to analyze the marine infauna.
- In September the Swedish Centre for Renewable Electric Energy Conversion was born and centered at the division for Electricity at the Ångström laboratory of Uppsala University.

2005

- A motor was connected to the laboratory generator in order to drive it at high speeds, while a buoy with a force sensor was installed at LRS.
- Five biology buoys were installed to study the environmental impact.
- The first WEC was built and named L1 (Lysekil 1).

2006

- At the beginning of 2006 a measurement station was built in the island of Härmanö.
- The first wave energy converter, L1, was installed on the 13th of March.

2007

- New biology buoys were put in place. At the end of May there were 21 buoys in the Lysekil Research Site.
- For the first time the WEC was run against a DC-load.
- An observation tower was erected near the research site.
- The wire of the L1 broke again in July.

2008

- To investigate the possibility of decreasing the peak forces on the generator, a ring shape buoy was attached to the L1 on the 21st of May.
- Biological studies were performed and design problems in biology buoys were found.
- A marine substation was tested in the lab of the Division for Electricity in June.
- On month later a networking camera was located in the observation tower in order to monitor the park directly from Uppsala University.
- Two new WECs, L2 and L3, were ready to be mounted.

2009

- The new WECs were installed in Lysekil during February.
- In March the substation was transported and assembled in LSR.
- L1, L2 and L3, were separately rectified and connected to a common DC-Bus in the substation. Then, the output power was converted back to AC with an inverter and transported into land.
- One new generator, L9, was launched.

2010

- In January, the wave measurement buoy communicated errors in measurements. The park was found full of ice.
- The number of biology buoys was reduced to two in April and increased to 18 between June and September.
- An electric component was installed to actively control the DC-voltage.
- In June, a new buoy made by Seabased was mounted on the L9. Then, this buoy was replaced with a ring one.
- A new circuit, called a resonance circuit, was connected to L9. It will be installed again in the summer 2011.
- In November 22, four generators were launched without buoys. They are L4, L5, L7 and L8.

The history of the Lysekil Research Site has shown a step by step development and improvement of the wave energy concept. Many important lessons have been learned as the researchers have faced the challenges of the oceans.

1.3.3 Environmental impact

The WEC technology is expected to have little or limited effect on the environment and it will contribute to fulfill some important environmental goals the Swedish Parliament approved [12, 13]:

- limited emission of greenhouse gases,
- fresh air,
- only natural acidification,
- protecting ozone layer,
- safe radiation environment.

Furthermore, this technology has been shown to provide a positive interaction between marine life and offshore structures (for more information see [9], [10] e [11]). The negative impact of the converters on the environment is related to the presence of hydraulic oil or poisonous paints in some wave energy technologies, dangerous substances for the marine life. The concept studied at the Lysekil Research Site does not contain those paints, being a very important part of the concept from the beginning. Besides, the biological growth can cause a negative impact on the converter, compromising the good operation of the system. This phenomenon is called biofouling and it depends on the types of organisms living all around the WEC, for this reason the intensity of the problem varies from one place to another in the world. Moreover, biofouling changes with depth: the greater the depth, the smaller the problem. On the other side, the impact of converters is positive since they serve as artificial reefs, promoting biodiversity, preserving old habitats and developing new ones. Figure 1.5 shows some organisms living on or around WECs in Lysekil Research Site.

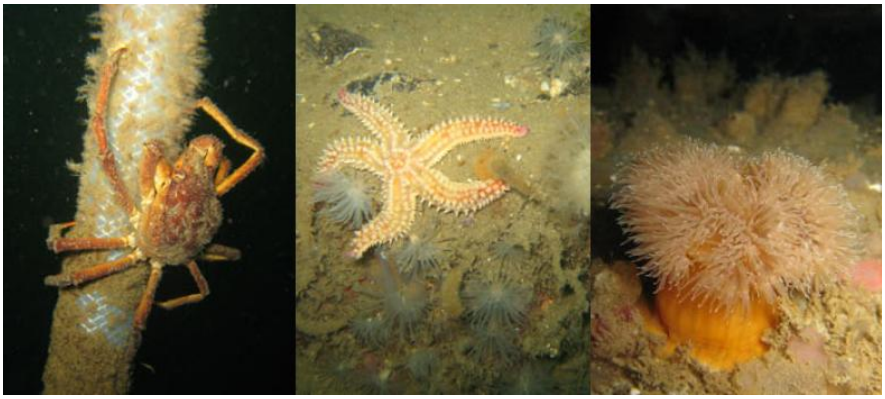

Figure 1.5: Biological life around the WEC, photographed by Kalle Haikonen.

Chapter 2

Theory

2.1 Linear theory of ocean waves

The linear theory of ocean waves assumes:

1. ideal and incompressible fluid,
2. irrotational fluid,
3. conservative field.

Called $\overline{v}$ the velocity vector and considering the previous hypothesis, the *continuity equation* becomes:

$$\nabla \bullet \overline{v} = 0$$

The assumption of irrotational fluid is verified if $\overline{v}$ admits a potential function, $\phi(x, y, z, t)$, whose gradient coincides with the velocity field, i.e.:

$$\overline{v} = \nabla\phi$$

The *continuity equation* is further simplified in the *Laplace's equation*:

$$\nabla^2\phi = 0$$

In order to solve this equation, the following boundary conditions are required:

1. sea floor boundary condition ($z = -h$)

$$-\phi_z = 0$$

2. cinematic surface boundary condition ($z = \eta(x,t)$)

$$\phi_z = \eta_x \phi_x - \eta_t$$

3. dynamic surface boundary condition ($z = \eta(x,t)$)

$$\eta + \frac{1}{2g}(\phi_x^2 + \phi_z^2) - \frac{1}{g}\phi_t = 0$$

Since the value of η is unknown and the conditions are not linear in ϕ and η, the problem can be simplified by neglecting non linear terms, which are small compared to the order of magnitude of linear terms. The new conditions are respectively:

1. $\phi_z = 0$, $z = -h$;
2. $\phi_z = -\eta_t$, $z = 0$;
3. $\eta = \frac{1}{g}\phi_t$, $z = 0$.

The last two equation can be merged in the single condition:

$$\phi_z + \frac{1}{g}\phi_{tt} = 0$$

The celerity is defined as

$$C = \frac{L}{T}$$

being L the wavelength and T the period. If $C = \frac{x_0}{t_0}$, i.e. $\frac{x_0}{L} - \frac{t_0}{T} = 0$, then $\eta(0,0) = \eta(x_0, t_0)$.
η can be expressed as function of the phase θ:

$$\theta = 2\pi\left(\frac{x_0}{L} - \frac{t_0}{T}\right) = kx_0 - \omega t_0$$

where k is the wave number and ω is the angular frequency. The next step is to eliminate the dependence of the equations from x and t. The *Laplace's equation* becomes:

$$\phi_{zz} + k^2\phi_{\theta\theta} = 0$$

while the surface boundary condition turns into:

$$\phi_z + \frac{\omega^2}{g}\phi_{\theta\theta} = 0$$

Now a solution for ϕ can be obtained, using the surface and sea floor boundary conditions, and the *Laplace's equation*:

$$\phi = \frac{a * g}{\omega}\frac{\cosh k(h+z)}{\cosh(kh)}\sin\theta$$

Finally, the *dispersion equation* can be calculated by replacing the last equation into the surface boundary condition:

$$\omega^2 = kg\tanh(kh)$$

Deep water

When the water depth is greater then one-half of the wavelength, $\frac{h}{L} > \frac{1}{2}$, the wave is classified as a deep water wave. Water particles inside this type of wave move forward and backward, up and down in a circular orbit whose diameter decreases with depth until it essentially disappears at the wave base.

Shallow water

When the depth is less then one twentieth of their wavelength, $\frac{h}{L} < \frac{1}{20}$, waves are said to be in shallow water. In this case, the water particle orbits inside the wave become elliptical rather then circular: the up-down component of the motion is squeezed by the presence of the bottom. The squeezing happens more quickly then the reduction of orbit size with depth, so that the resulting configuration is the one shown in Figure 2.2.

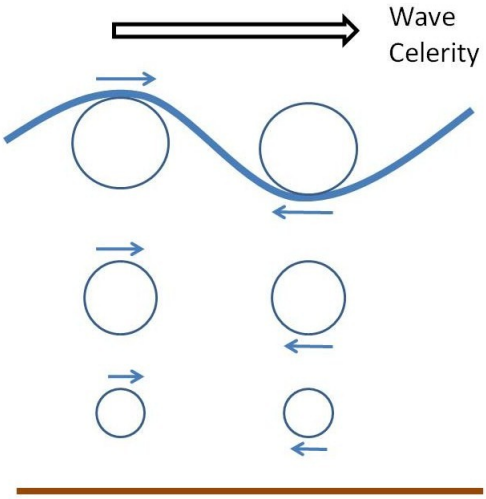

Figure 2.1: Water particle orbits in deep water.

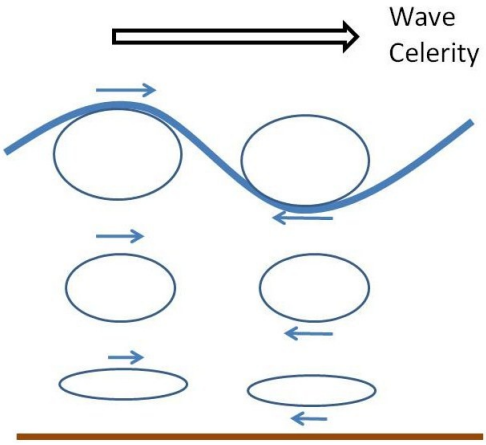

Figure 2.2: Water particle orbits in shallow water.

Wave celerity

The speed at which an individual wave form propagates is known as the wave celerity. For a deep water wave the celerity is directly proportional to the wave period, T. The formula for deep water celerity (m/sec) is:

$$C = \sqrt{\frac{g}{k}} \approx 1.56T$$

The celerity of an individual shallow water wave, C, is given by the formula:

$$C = \sqrt{gh}$$

where h is depth and g is the acceleration of gravity. Note that the deep water wave celerity does not depend on water depth, while the shallow water celerity depends on depth rather then wave period.

Long waves

Tide waves are clearly shallow water waves. By definition $C = \frac{L}{T}$, hence, for a shallow water wave:

$$L = TC = 3.13T\sqrt{h}$$

The dominant period of the semi diurnal tide being 12.42 hours and the greatest ocean depths being about 12,000 meters, the corresponding tidal wavelength would be 15,330 km. One twentieth of this value is 767 km. In other words, tide waves are way too long to even approach the limit where they would not be classified as shallow water waves [17]. In fact, their length-to-depth ratio is so extreme that the vertical motion of the water particles is insignificant compared to their horizontal motion as shown in Figure 2.3. The horizontal motion on the other hand is quite significant as it represents the tidal current.

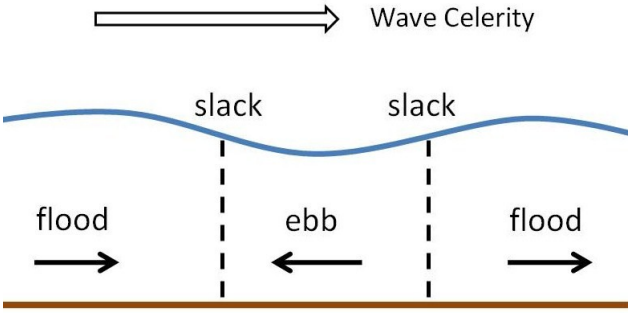

Figure 2.3: Shallow water waves.

2.2 Theory of tides

Tides are the periodic rise and fall of the water level in seas and oceans, and they are the result of the gravitational pull of the Moon and Sun on the Earth, as well as the perpetual spinning rotation of the Earth itself.

2.2.1 Lunar and Solar tides

The largest influence is the gravitational effect of the Moon: the water is pulled toward the Moon itself and a bulge is made on the surface of the ocean at the side of the Moon. Furthermore, the spinning of the Earth-Moon system causes a centrifugal force creating a second bulge. These bulges are high tides. As the Moon rotates around the Earth the bulges shift with it causing a shift in the water level. The Moon rotates in the same direction the Earth rotates around its axis, thus the Moon takes a little more then a day, 24 hours and 50 minutes, to fully rotate around the earth. Moreover, the effect of the Moon is the same both in the zenith and nadir, so one tide cycle takes about 12 hours and 25 minutes and the time between a high tide and a low tide is, on average, 6 hours and 12.5 minutes. This explains why tides arrive at the same location almost an hour later each day. Conversely the tidal effect due to the Sun that exercises a gravitational attraction on the Earth, is less powerful then the lunar effect. Although the distance between Earth and Sun is three orders of magnitude greater then the distance Earth-Moon, the Sun's mass is five orders of magnitude higher then the Moon's mass, so the Sun's contribution is not negligible. Approximately twice a month, the Sun, Moon and Earth will more or less align to

form either a Full Moon or a New Moon. During each phase of a New Moon or a Full Moon, the sum of the two tidal effects results in higher high tides and lower low tides, both called *Spring Tides* (see Figure 2.4), a term derived from the springing up of the water. Twice each month the Sun and Moon are at right angles to the

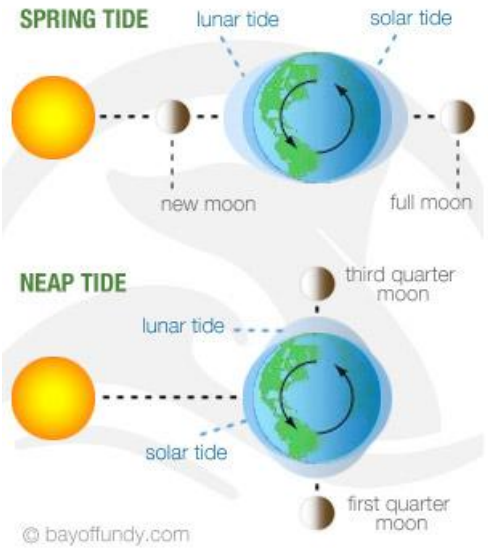

Figure 2.4: Spring and Neap Tides.

Earth and opposing each other (First and Third Quarter Moons). In that case the tidal ranges are less then normal and they are called *Neap Tides*. Because of these periodic fluctuations in gravitational pulls from the Sun and Moon, the hight of the tides varies from day to day [14].

2.2.2 Acting forces

In this section, the forces acting on the unit mass of water on Earth's surface are analyzed according to the static theory, based on the assumptions listed below:

- single interaction between Earth and Moon,
- Earth covered by an uniform layer of water,
- conditions of static equilibrium,
- neglect:

- Coriolis force,
- conformation of the ocean floor,
- presence of continental masses,
- inertia, friction and resonance.

With reference to Figure 2.5 the following forces are listed:

1. f_c, the centrifugal force in the direction parallel to the line joining the centers with sense from the Moon to the Earth;
2. f_a, attraction of the Moon toward the center of itself;
3. f_g, attraction of the Earth toward the center of itself;

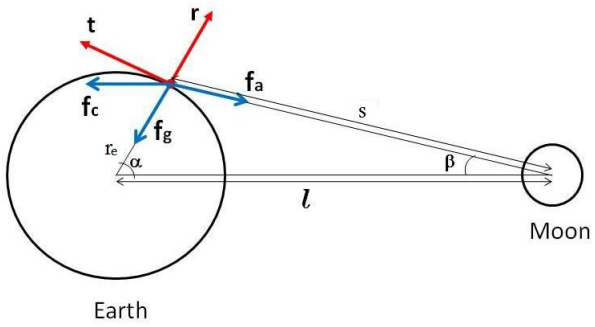

Figure 2.5: Forces acting on the unit mass of water on Earth's surface.

In static conditions, the centrifugal force will be balanced by the gravitational one and the static equilibrium can be expressed as:

$$M_{e,m}\omega^2 l_{e,m} = G\frac{M_m M_e}{l^2}$$

with

M_m = Moon's mass,

M_e = Earth's mass,

ω = angular velocity of relative revolution,

$l_{e,m}$ = distance between the common axis of revolution and the Earth/Moon's center,

G = gravitational constant,

l = distance between Moon and Earth's centers.

This being stated, the following equations are obtained:

$$f_c = \omega^2 l_e = G\frac{M_m}{l^2} = g\frac{r_e^2}{M_e}\frac{M_m}{l^2} = g\frac{M_m}{M_e}\left(\frac{r_e}{l}\right)^2$$

$$f_a = G\frac{M_m}{s^2} = g\frac{M_m}{M_e}\left(\frac{r_e}{s}\right)^2$$

where s is the distance between the unit mass of water and the Moon,

$$f_g = g$$

because the attraction Earth-oceanic mass is predominant.
Projecting these forces in the radial and tangential directions:

$$F_r = -f_g - f_c\cos\alpha + f_a\cos(\alpha+\beta) \approx -g$$

$$F_t = f_c\sin\alpha - f_a\sin(\alpha+\beta) \approx -\frac{3}{2}g\frac{M_m}{M_e}\left(\frac{r_e}{l}\right)^3\sin\mathbf{2}\alpha$$

As highlighted, the frequency doubles, which is why the tide's cycle is about 12 hours.

2.2.3 Configuration of free surface

The configuration of the water surface is obtained by imposing the orthogonality condition:

$$\frac{d\eta}{dx} = -\frac{F_t}{F_r} = \frac{3}{2}\frac{M_m}{M_e}\left(\frac{r_e}{l}\right)^3\sin 2\alpha$$

The solution to this equation is approximately:

$$\eta = \frac{r_e}{4}\frac{M_m}{M_e}\left(\frac{r_e}{l}\right)^3[3\cos 2\alpha + c]$$

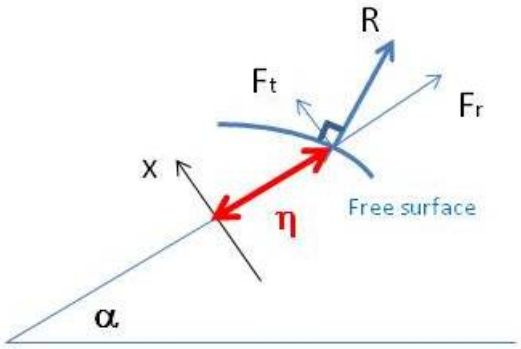

Figure 2.6: The configuration of the water surface imposing the orthogonality condition.

This is the equation of a spheroid with major axis directed toward the Moon. Changing the value of α in the previous equation, the position of the free surface is obtained and its excursion is included between 36 cm and -18 cm. Moreover, if the actual declination of the Moon is considered, it can be shown that daytime tides prevail with increasing latitude. The effect of the solar attraction is not negligible, as already said, and it can be proved through a rough calculation by including the mass of the Sun instead of the mass of the Moon to get:

$$\frac{\eta_s}{\eta_m} \approx 46\%$$

Of course this is not an exact theory, but it helps to better understand the problem. The limits of the static theory are essentially three:

1. errors in the phase of the tides,

2. deformation of the tidal waves in the presence of continents,

3. resonance effects in closed basins.

2.2.4 Water level measurement

The measurement of tides is not quite direct: the initial data recorded are really water level measurements. An instrument called tide gauge automatically records water levels at fixed intervals of time. These data have to be analyzed before making use

of them, because it's easy to produce bad water level records. Every measurement station requires the following components:

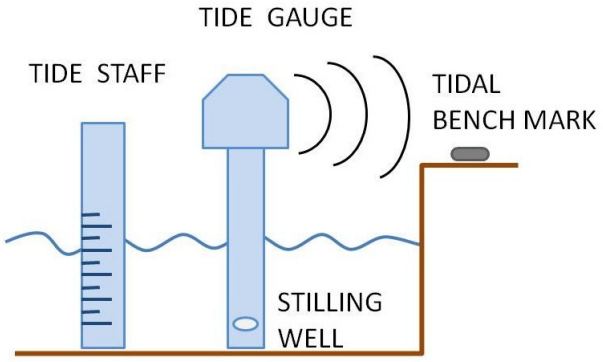

Figure 2.7: Water level measurement, tide gauge.

1. Tide Staff. Graduated in feet or centimeters, it is installed in a permanent housing. The zero mark on the staff becomes the vertical reference that all recorded water levels refer to. The staff is insurance against gauge disturbance or malfunction.

2. Tidal Bench Mark. After a leveling survey between the mark and the staff, a permanent mark such as a brass disc set in concrete prevents the loss of the station datum (tide staff zero) if anything happens to the staff. For this reason, the bench mark is insurance against damage to the staff.

3. Tide Gauge. This device could be mechanical or acoustic and it is used for recording water level. The acoustic water level meters, that measure and record data electronically, are replacing the mechanical ones. While the mechanical gauge features a spring-loaded pulley and wire leading down to a cylindrical float inside a vertical stilling well, the acoustic devices utilize an acoustic shock-wave sent down a vertical wave-guide. After striking the water surface, the wave is reflected back to a transducer and microcomputer that converts travel time to distance based on the speed of sound in air. Of course, any gauge needs to be monitored frequently to avoid systematic errors in the time or hight recorded.

4. The Stilling Well. It is a tube or pipe of fixed inside diameter designed to admit only low-frequency oscillations in water level inside the sensing environment. The bottom of the tube is usually sealed except for a single small orifice that limits the rate at which water can enter or exit the tube.

2.2.5 Tides around the world

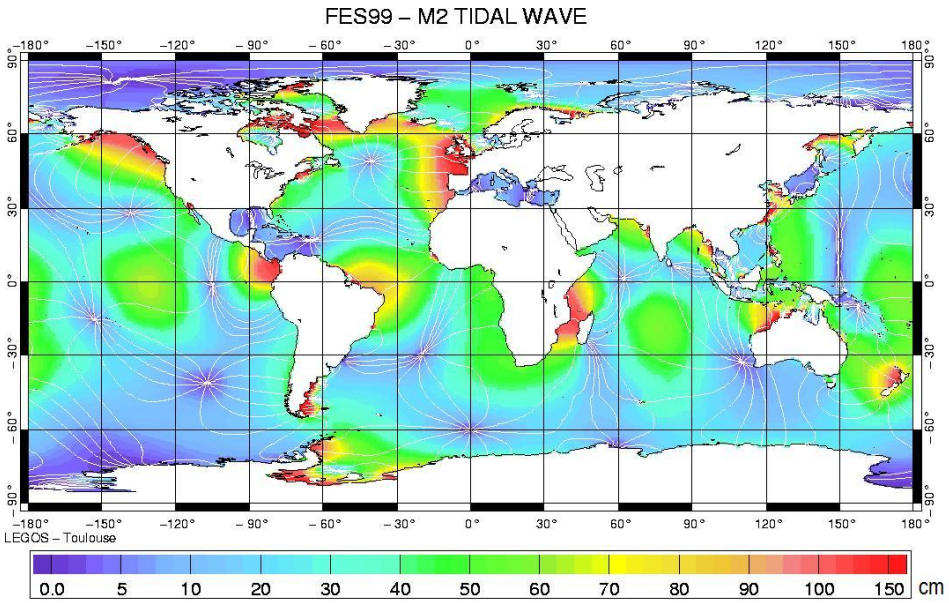

Figure 2.8: Global map of tidal waves calculated from satellite altimeter observations of the height of the sea surface assimilated into a numerical model of the tides. Full lines are contours of constant tidal phase, contour interval is 30°. Colors give tidal amplitude, contour interval is 10 cm. (Credits CLS /Legos).

Wave propagation, tidal amplitude and period vary from one place of the globe to another depending on the bathymetry, the coastal geometry, Coriolis forces and other complex parameters. In some areas, waves generated from the breakdown of tides have to be taken into account, see Figure 2.8.

Scandinavian tides

The Skagerrak and Kattegat (Figure 2.9) are seas on the west coast of Sweden where Lysekil is located. They are characterized by semi-diurnal tides whose amplitudes are around 10 and 5 cm respectively.

Figure 2.9: Skagerrak and Kattegat seas. The red dot indicates where Lysekil is located.

During spring tides, the amplitude can rise to 40 cm in the Skagerrak and 20 cm in the Kattegat. On the east coast of Sweden, the Baltic Sea is too small to have own significant tides and it is not influenced by the North Atlantic tides as it happens to the Skagerrak and Kattegat. Actually, tides are created in the Atlantic Ocean and they propagate as long waves into the Norwegian Sea. One part of the waves propagate along the coast, while another part turns in the North Sea and it is reflected northwards again. The tidal pattern gets complicated and it gets worse because of the influence of varying depths, irregular coastlines and rotation of the earth [16]. In order to have an idea about water level averages and monthly tides registered in a Norwegian port, see Figure 2.10 and 2.11 respectively.

Year	Mean	Jan	Feb	Mar	Apr	May	Jun	Jul	Aug	Sep	Oct	Nov	Dec
2010	116	114 31	114 27.06	117 31	111 30	105 31	102 30	114 31	119 31	120 30	133 31	124 30	117 31

Figure 2.10: Statistics showing monthly and annual water level averages in the port of Ålesund. The mean values are given in cm relative chart datum - Mean / no. of days.

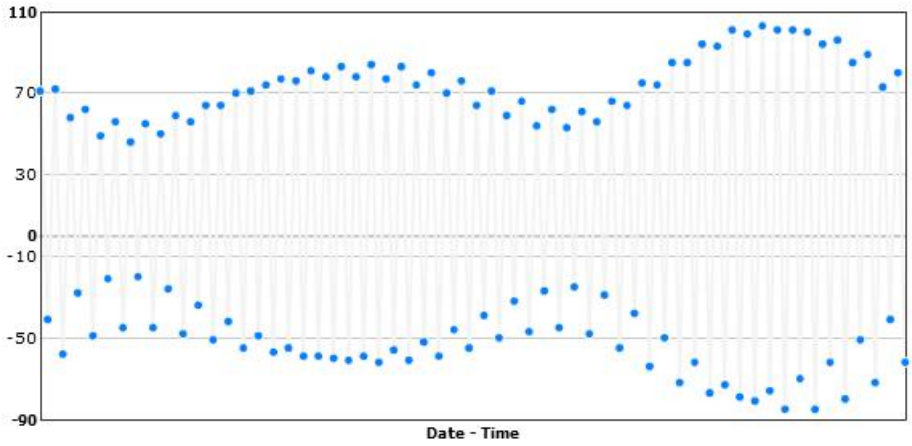

Figure 2.11: Predicted tide table for Ålesund during november 2011 according to the Norwegian Hydrographic Service. The heights on the y-axis are given in cm above mean sea level. Time zone is GMT + 1 hour in the winter time.

Mediterranean tides

Mediterranean tides generate a mean variation of about 40 centimeters. Headwinds or, more often, higher-then-normal atmospheric pressure attenuate the effect of these tides, sometimes making them virtually impossible to see. For this reason people associate the Mediterranean with small tides. In the Adriatic and south of Sicily tides are very small in the vicinity of amphidromic points where the tidal range is zero, as shown in Figure 2.12. The Atlantic affects tides in the Strait of Gibraltar, but its influence soon declines further east. Conversely, the range could be very high, e.g. in the Gulf of Gabes off the coast of Tunisia: the range reaches almost two meters [15].

2.3 3D CAD Design with SolidWorks

SolidWorks is a 3D mechanical CAD program developed by Dassault Systèmes SolidWorks Cop. since 1995, and its logo is shown in Figure 2.13. This solid modeler utilize a *parametric feature based approach* to create models and assemblies, i.e. the dimensions and the relations drive the geometry. The shape and the geometry of an assembly are determinate by the values of constraints to which parameters are referred. Parameters can be either numerical, like

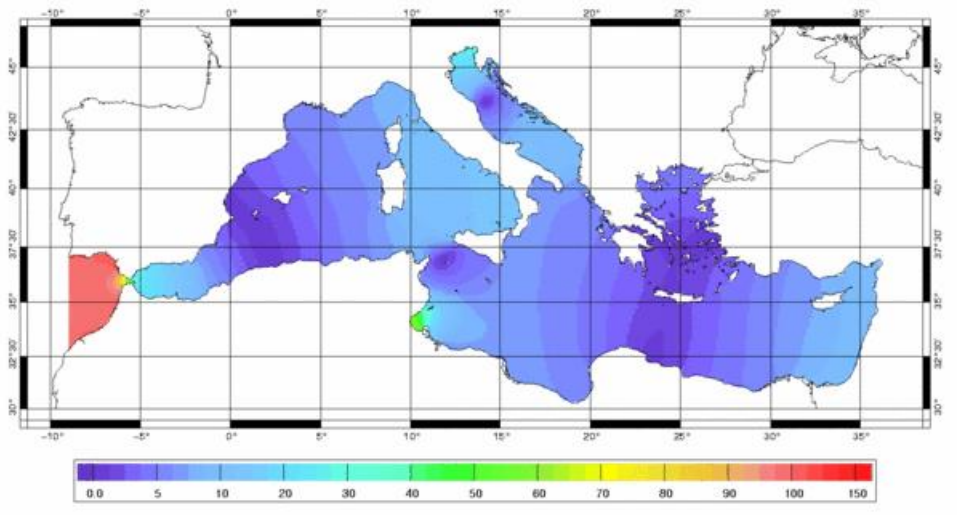

Figure 2.12: Amplitude (in cm) of the principal lunar tide in the Mediterranean predicted by the CEFMO model (release 2000). (Credits Legos).

Figure 2.13: SolidWorks Premium 2010, version used to design the model.

lengths or diameters, or geometrical, like tangent, parallel, concentric, etc.

A 2D sketch is the first step to design an object. It consist of points, lines, arcs, an other geometrical entities, and splines. Dimensions are used to define the size of the sketch, while relations to define attributes. Once the object is ready, it can be used as a part of a more complex model, the assembly, that is mounted thanks to the use of mates. Assembly mates define relations of tangency, parallelism, concentricity with respect to different parts. In order to know how the model behaves as a physical object, a design validation tool, called SolidWorks Simulation, is added to the standard design application. It is based on Finite Element Analysis, FEA, a numerical technique of solving problems described by a set of partial different equations. This tool allows to carry out structural, thermal, acoustic analysis starting from the geometrical

model. The model, either a part or an assembly, must be characterized by:

(a) material properties;

(b) applied loads;

(c) restrains.

Then, the model is discretized into small and simply-shaped entities, the finite elements. This process is known as meshing and the result depends on the size of these elements. After the preprocessing, the desired results such as stress and displacement are computed. Results have to be analyzed in the post processing step, and their veracity must be evaluated.

2.4 Control System with LabVIEW™

LabVIEW is a program development application, like various commercial C or BASIC development systems, but it does not use text-based languages to create lines of code: it uses a graphical programming language (Figure 2.14). In fact, LabVIEW relies on graphical symbols rather then textual language to describe programming actions, using icons and terminology familiar to scientists and engineers.

Figure 2.14: LabVIEW icon, by National Instruments.

LabVIEW includes libraries of functions and development tools designed specifically for instrument control. Its programs are called virtual instruments (VIs)

because their appearance and operation imitate actual instruments. A VI contains three components [18].

- Front panel, which serves as the user interface. The front panel is built with controls and indicators, which are the interactive input and output terminals of the VI, respectively.
  - Controls are knobs, push buttons, dials, and other input devices. Controls simulate instrument input devices and supply data to the block diagram of the VI.
  - Indicators are graphs, LEDs, and other displays. Indicators simulate instrument output devices and display data the block diagram acquires or generates.
- Block diagram, that contains the graphical source code which defines the functionality of the VI. After the front panel has been built, it is possible to add code using graphical representations of functions to control the front panel objects. It's possible to insert four components in the block diagram:
  - terminal, that represents the data type of the control or indicator, in other words it's the entry or exit port which exchanges information between the front panel and block diagram;
  - node, analogous to statement, operator, function, and subroutine in text-based programming languages;
  - wire, used to transfer data among block diagram objects;
  - structure, used to repeat blocks of code and to execute code conditionally or in a specific order.
- Icon and connector pane, which identify the VI, so that a VI can be used in another VI. A VI within another VI is called a sub VI. A sub VI corresponds to a subroutine in text-based programming languages. An application is divided into a series of tasks, which could be divided again until a complicated application becomes a series of simple subtasks.

The Figure 2.15 presents a simple VI that allows to add or subtract two variables.

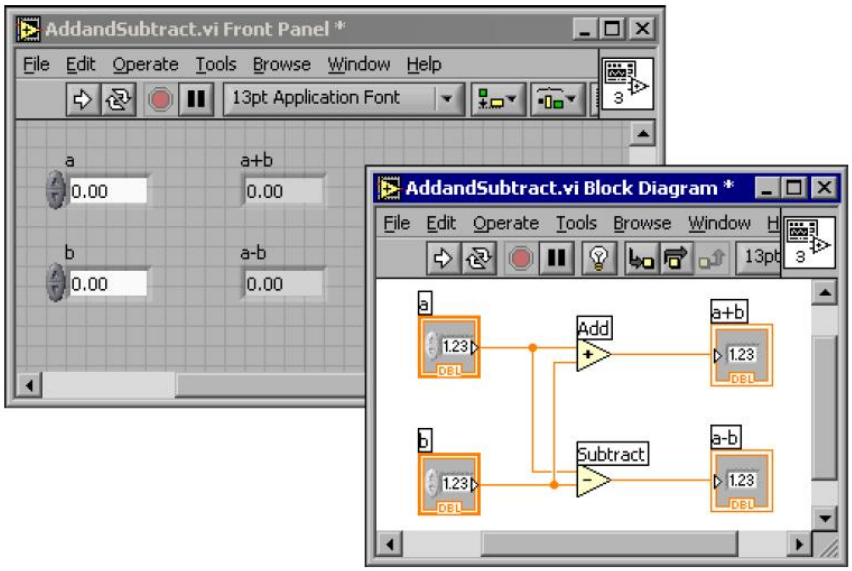

Figure 2.15: Example of a block diagram and its corresponding front panel

In order to set several work environment options, the Controls and Functions palettes are used. The Controls palette is available only on the front panel and contains the controls and indicators, while the Functions palette is available only on the block diagram and contains VIs and functions used to build the block diagram. Clicking an object on the palette, the object can be dragged and dropped on the front panel or block diagram. The menu and toolbar items are useful to operate and modify panel and diagram objects.

Chapter 3

Experimental work

During the Spring of 2010 a group of students from Uppsala University started to brainstorm about possible solutions to minimize the tidal effect on point absorbers [19]. The most suitable solution they found is the one shown in Figure 3.1.

The rope that leads down to the generator is attached to a screw, which runs inside a gear that has internal threads like a nut. The gear is connected to the engine through another screw, called worm. When the engine is set in rotation, the screw moves up or down according to the spin direction of the motor.

This solution is the starting point of the thesis: a device that works with the

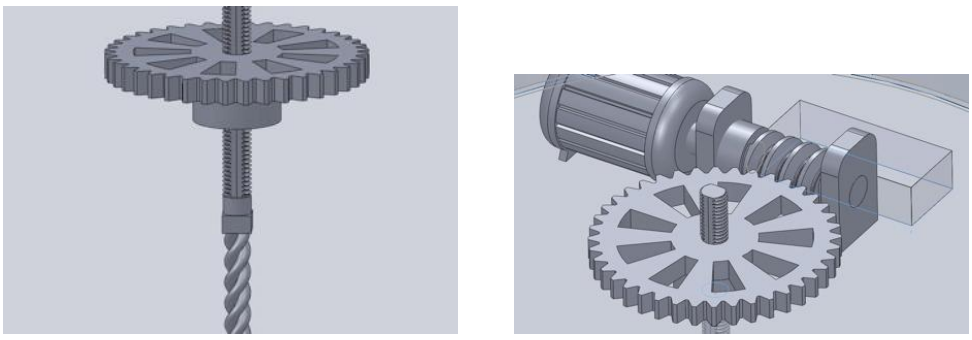

Figure 3.1: On the left the cable that connects the buoy to the generator is attached to a screw running through a gear [19], on the right overview of the worm gear and the motor.

same principle is designed, built and tested on a small-scale point absorber. The current chapter describes how these goals have been achieved.

3.1 Small scale model

First of all, a reference tide is chosen: the one measured in Ålesund, Norway, has been selected. According to the Norwegian Mapping Authority the amplitude of this tide is about 1 m. The reason why the Norwegian tide has been selected is due to the simple fact that a full scaled version of the buoy presented in this thesis could be tested there.

The second step is to choose the scale of the problem. It has been reduced to one-tenth of the reality, so that a tide's cycle in the lab can be simulated by changing the water level in the range of ± 10 cm, where 0 represents the average water level. This means that the length of the rope changes by 20 cm during a complete cycle. The model realized in SolidWorks is shown in Figure 3.2 and a thorough description of its components is given below.

The standard screw selected is a TR10x3, where TR stands for trapezoidal threads, 10 is the nominal diameter in mm, and 3 is the pitch in mm, see Figure 3.3. Trapezoidal threads convert circular motions in linear motion and they are mainly used for linear drives. The nut and the cogwheel merge in a single component in order to save space and work. Steel is used for making the screw and the worm and bronze is used for the nut. The steel has got a remarkable mechanical strength, while the bronze has got good wear resistance and low friction coefficient in the coupling screw-nut. These components are collected in a plastic housing that is provided with four bearings; two principal bearings concentric with the screw and two lateral bearings concentric with the worm.

The motor is connected to the device by pushing its shaft into the inner hole of the worm, as shown in Figure 3.6. As the motor's shaft move, the worm turns forcing the nut to rotate. Every twenty revolutions of the nut, the screw is displaced by 3 mm. The screw goes up or down depending on the direction

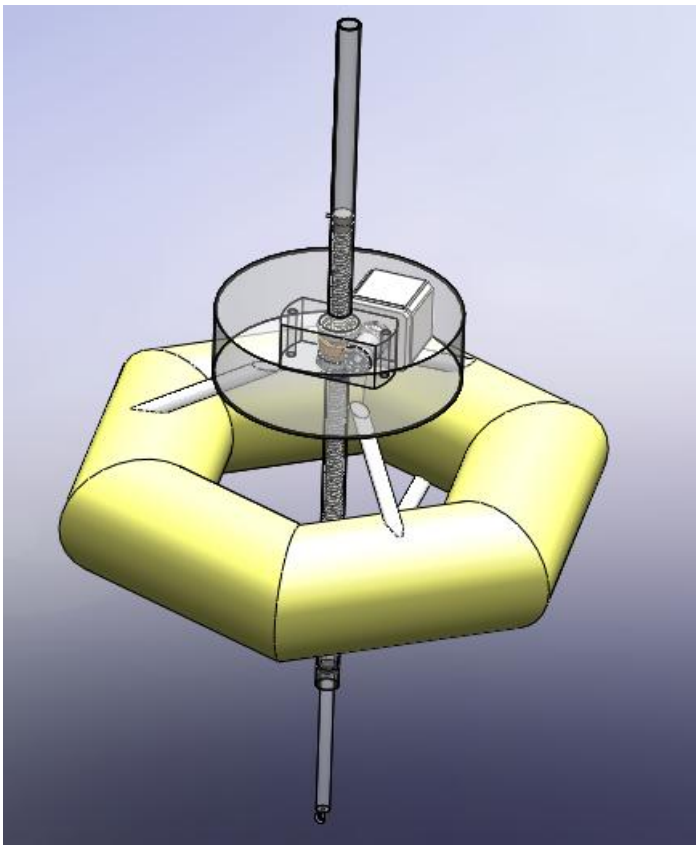

Figure 3.2: Small-scale model drawn with SolidWorks.

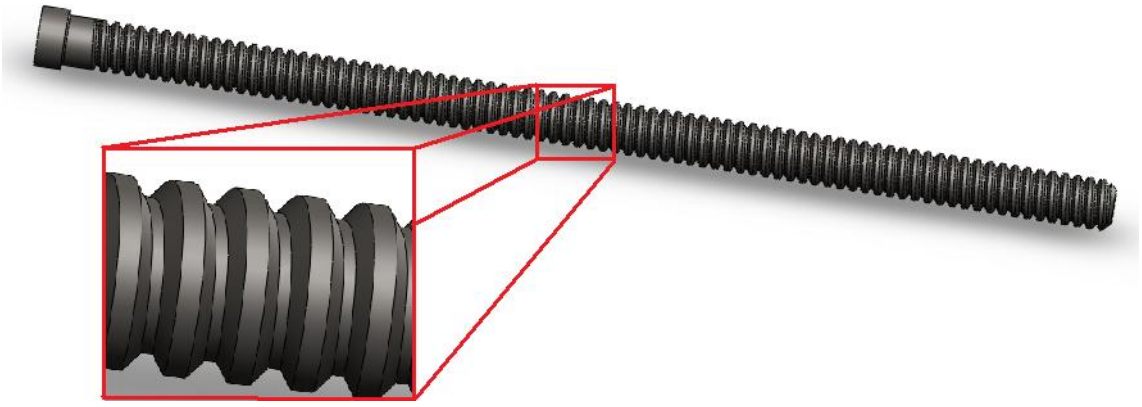

Figure 3.3: TR10x3 screw, 20 cm long.

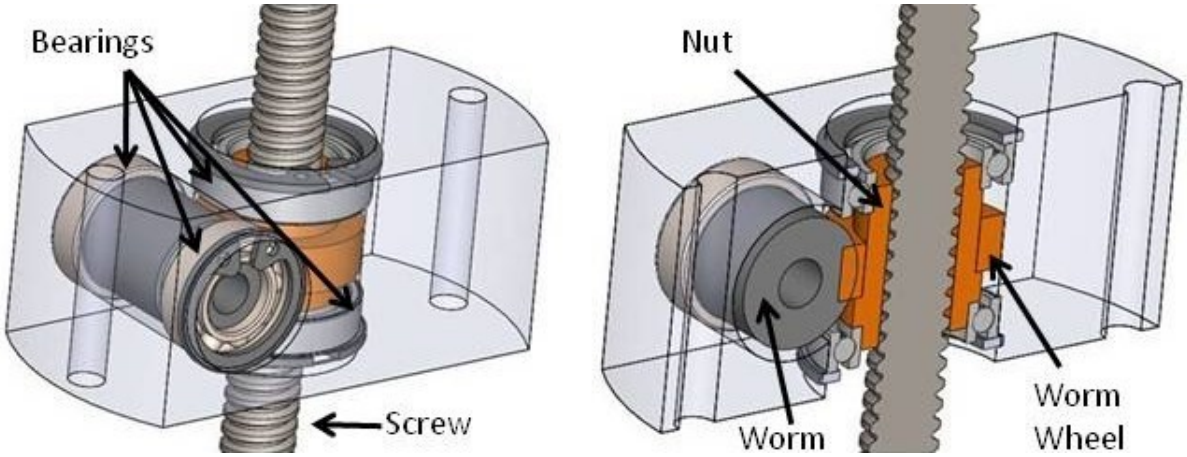

Figure 3.4: The device that moves the screw is shown on the left, while a section of the device is displayed on the right.

Figure 3.5: Pictures of the virtual and real device.

of the motor, counterclockwise or clockwise respectively.

The device and the motor are located in an external plastic housing which protect them from the water. In the real case it will be a protection from wind, rain, sun and other exogenous effects, while a light to detect the position of the buoy will be placed on the upper pipe.

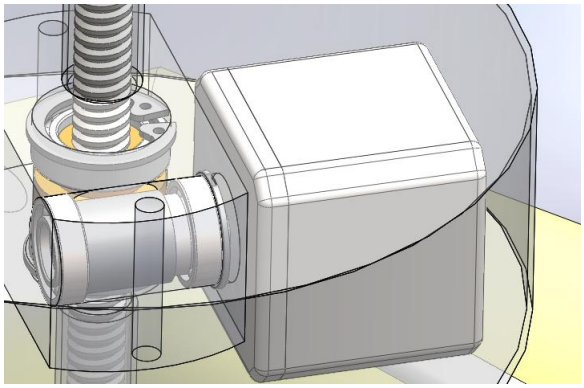

Figure 3.6: The motor is connected to the device and protected by a plastic housing.

To avoid the infiltration of water from the bottom, a seal and a piston are used (see Figure 3.7): the seal is situated in the lower pipe and the piston is attached to the screw. The seal chosen is an U-seal made of NBR (Nitril rubber). U-seals have high dynamic sealing effect and excellent resistance to abrasion.

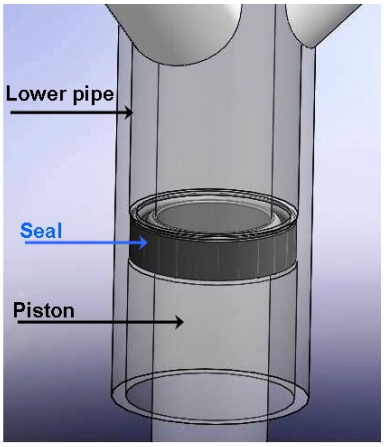

Figure 3.7: A U-seal is used to avoid infiltration of water from the bottom.

The plastic structure is mounted on the buoy through six small pipes glued with epoxy resin to ensure high resistance. The buoy is made of polystyrene

and it is covered with one layer of glass fiber and epoxy resin in order to make it waterproof (Figure 3.8).

Figure 3.8: Polystyrene before and after the application of the fiberglass.

Epoxy resin

The epoxy resin is a very versatile plastic. It is possible to buy it as a liquid in two containers, see Figure 3.9, one for the resin and the other for the liquid hardener. A chemical reaction takes place when they are mixed in the correct proportions, producing an hard tough transparent plastic. In combination with glass fiber it makes a very strong glass reinforced plastic laminate, i.e. fiberglass. It is mostly used in the construction and repair of high-performance sailing boats and is an excellent resource for wooden or GRP (Glass-reinforced plastic) boat maintenance. It is really simple to use, but at the same time it is important not to neglect basic safety requirements for working with these materials. The resin can be carcinogenic if digested or if it comes in contact with the skin. Rubber gloves, spectacles, safety clothing and mask have to be worn. Furthermore, it is advisable to work outdoor to disperse fumes and particles. The surface that is to be reinforced must be dry and at a comfortable temperature (about 15 - 20 degrees Celsius). Then, one part of hardener is mixed with five parts of resin. The tool used for measuring the resin should not be used for the hardener and vice versa. The curing process generates a lot of heat and poisonous fumes can be produced. In order to avoid these side effects is better to use a wide container and to mix a small quantity of products

at a time. Also, it is good to remember that there is only a limited amount of time available before the curing process makes the mixture unusable: the mixture remains usable for about 10-15 minutes at room temperature. The surface has to be covered with the glass fiber, fixing it with the epoxy resin. A careful cleaning of the brush and the container with acetone is necessary for the tools to be usable for the next use. After six hours the resin will have cured to a hard plastic and further hardening will continue for 5-7 days, until full strength is attained.

Figure 3.9: Epoxy resin and hardener used to make the buoy waterproof.

3.1.1 Buoyancy

For the purpose of dimensioning the floater of the model, the buoyancy of the system was calculated. According to the Archimedes' principle, this system is buoyed up by a force equal to the weight of the fluid displaced by the small-scale model. The buoy floats if the weight force, F_{buoy}, is lower then the Archimedes' force, F_{arch}. The following equations are used to demonstrate that the model does not sink:

$$F_{buoy} = W_{buoy} * g$$

$$F_{arch} = \rho_w * V_{buoy} * g$$

$$\%V_i = \frac{\rho_{buoy}}{\rho_w}$$

with W_{buoy} being the weight of the model, ρ_w the water's density and ρ_{buoy} the buoy's average density, V_{buoy} the model's volume, $\%V_i$ being the percentage of immersed volume.

Table 3.1 shows that $F_{buoy} < F_{arch}$ and the immersed volume is about 56% of the model's total volume.

$W_{buoy}[kg]$	1.8
$F_{buoy}[N]$	17.7
$\rho_w[kg/m^3]$	1010
$V_{buoy}[m^3]$	0.003
$F_{arch}[N]$	31.8
$F_{res}[N]$	0
$\%V_i$	56

Table 3.1: Buoyancy of the small-scale model.

During the experiment conducted in the lab's tank the water level changes continuously, while the motor is activated after a fixed interval of time. Moreover, the buoy is fixed to the floor, because the generator is absent. For these reasons, the immersed volume of the buoy is not constant, neither is the Archimedes' force. This means that the wire is subjected to a force, F_{wire}, that changes with time. In order to have an idea of the importance of this variation, Table 3.2 was filled in. The model was virtually immersed of one centimeter every time (see Figure 3.10) and an increasing value of immersed volume, V_i, was calculated. The Archimedes' force is proportional to the variation of V_i, hence F_{wire} can be estimated.

$I_{buoy}[cm]$	$V_i[\%]$	$V_i[mm^3]$	$F_{arch}[N]$	$F_{wire}[N]$
0	56	1782178	17.7	0.0
1	71	2281488	22.6	4.9
2	85	2718357	26.9	9.3
3	93	2980671	29.5	11.9
4	93	2986314	29.6	11.9
5	93.3	2992091	29.6	12.0

Table 3.2: The variation of F_{wire} is calculated by changing the value of the buoy's immersed volume.

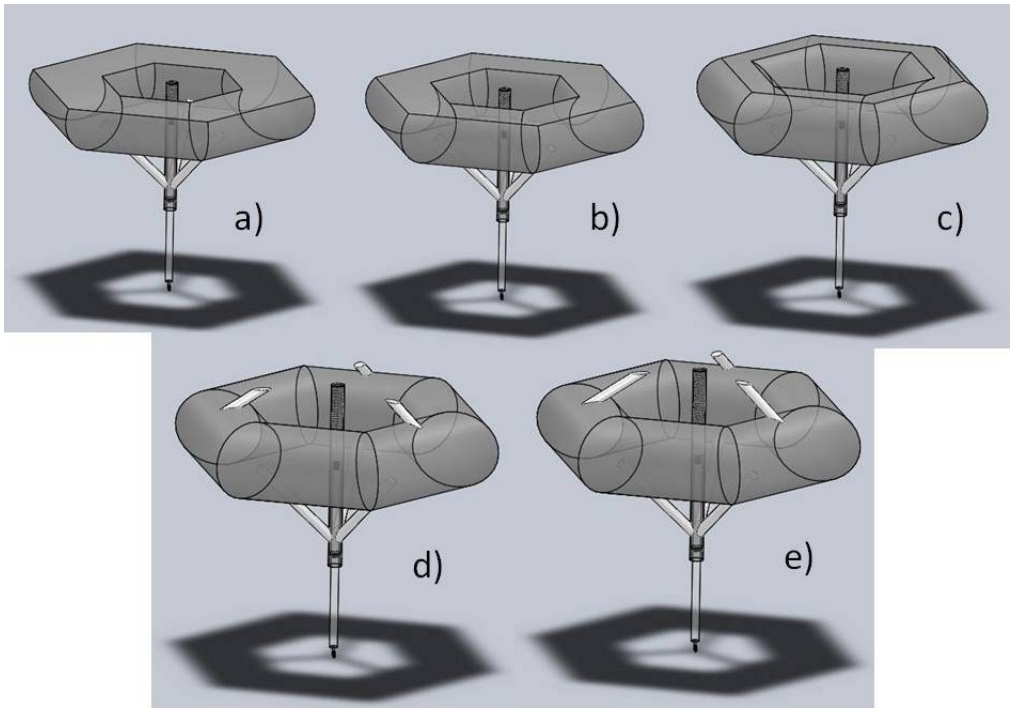

Figure 3.10: The model is sliced using SolidWorks, in order to calculate the immersed volume every time the water level increases by one centimeter.

3.1.2 Friction and torque

A way to calculate the torque required to lift or lower a load is presented here. Imagine that the nut is an inclined plane and the screw is a block to be pushed up to the plane, the nut forms a right angled triangle whose base is πD long and the hight is the pitch, see Figure 3.11.

The forces acting on the free-body diagram are:

(a) the force of the load directed downward,

(b) the normal force perpendicular to the hypotenuse of the triangle,

(c) the frictional force directed in the opposite direction of the direction of motion,

(d) an imaginary effort force acting in the direction opposite the direction of the frictional force.

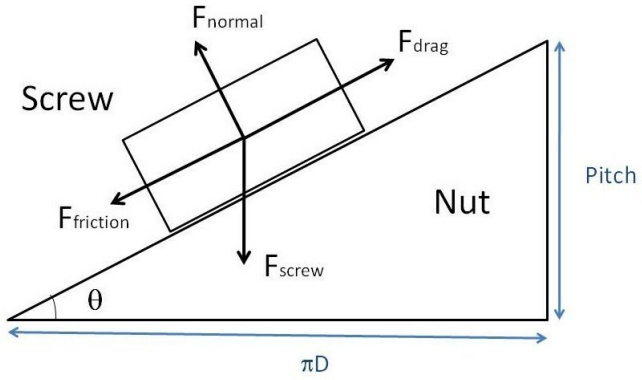

Figure 3.11: The nut threads are wrapped up into an inclined plane and the screw is considered as a block on that plane. The base of the inclined plane is one revolution of the nut long (πD).

The first step is to determine the friction force, given by:

$$F_{friction} = F_{normal} * \mu$$

where μ is the friction coefficient. For a steel screw and a bronze nut, the range of values of μ is 0.15-0.20 for the dynamic friction coefficient and 0.20-0.25 for the static one [21]. F_{normal} is given by:

$$F_{normal} = F_{screw} * \cos\theta$$

where θ is obtained as:

$$\theta = \tan^{-1}\left(\frac{Pitch}{\pi D}\right)$$

F_{screw} is the force of the load directed downward due to the weight of the screw, the weight of the piston and the Archimedes' force. In the ideal case, the screw is not subject to any external force but the weight force of the system piston-screw, m_{ps}:

$$F_{screw} = m_{ps} * g - \rho_w * V_i * g$$

where V_i is the immersed volume of the system piston-screw. During normal

operation conditions and in the worst case scenario, the screw is in the highest position allowed, so that the Archimedes' force is negligible:

$$F_{screw} = m_{ps} * g$$

The drag force, F_{drag}, required to continue pulling up the screw with constant velocity after it reaches the operating speed is given by:

$$F_{drag} = F_{screw} * \sin\theta + F_{friction}$$

The required torque that has to be applied to the screw to generate the force F_{drag} is obtained by:

$$M = \frac{F_{drag} D}{2\cos\theta}$$

In Table 3.3 the data used to solve the equations are listed, while in Table 3.4 and 3.5 results are summarized.

This being stated, the moment the engine must deliver to the worm in order to provide the screw with the torque M, has to be calculated.

D_{screw} $[m]$	0.008
P_{screw} $[m]$	0.003
μ_1	0.15
μ_2	0.25
m_{ps} $[kg]$	0.118
g $[m/s^2]$	9.81

Table 3.3: Data referring to screw and nut.

θ $[°]$	6.8
F_{screw} $[N]$	1.2
F_{normal} $[N]$	1.1

Table 3.4: Results for the system screw-nut.

The approach to calculate the torque for the worm wheel is similar to the calculations made for the screw. The same principle has been applied but in this case the worm is simplified as the inclined plane and the tooth of the

	μ_1	μ_2
$F_{friction}$ $[N]$	0.17	0.29
F_{drag} $[N]$	0.31	0.42
M $[Nm]$	0.001	0.002

Table 3.5: Results for the system screw-nut.

worm wheel as a block, as shown in Figure 3.12.

The force F_k operating in the contact area between the gears and the worm, see Figure 3.13, is given by:

$$F_k = \frac{M}{r_k}$$

where r_k is the worm wheel radius. The other forces acting are, as before:

$$F_{normal} = F_k * \cos\theta,$$

$$F_{drag} = F_k * \sin\theta + F_{friction},$$

The torque M_s the engine has to deliver is determined by the torque M associated to the screw:

$$M_s = \frac{F_{drag} D_s}{2\cos\theta}.$$

where D_s is the worm's diameter. Taking into account the data of Table 3.6, the results are summarized in Table 3.7.

r_k $[m]$	0.01
P_{cog} $[m]$	0.003
D_s $[m]$	0.01
θ $[^\circ]$	5.5

Table 3.6: Data referring to worm wheel and worm.

Another important variable that needs to be calculated is the efficiency of the inclined plane, whose value allows to demonstrate that the device is self-

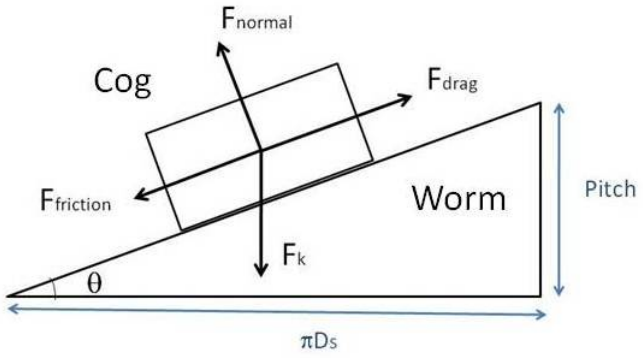

Figure 3.12: Schematization of the worm wheel (cog) and the worm.

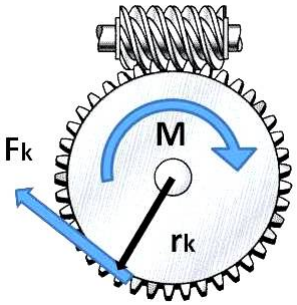

Figure 3.13: Force and torque operating between the worm and the worm wheel.

	μ_1	μ_2
F_k $[N]$	0.12	0.17
F_{normal} $[N]$	0.12	0.17
$F_{friction}$ $[N]$	0.02	0.04
F_{drag} $[N]$	0.03	0.06
M_s $[Nm]$	0.0002	0.0003

Table 3.7: Results for the worm.

locking. The efficiency is expressed as:

$$\eta = \frac{F_{load} \sin\theta}{F_{load} \sin\theta + F_{friction}} = \frac{\sin\theta}{\sin\theta + \mu * \cos\theta} = \frac{\tan\theta}{\tan\theta + \mu}$$

The friction coefficient μ can be written as $\tan\phi$, where ϕ is the friction angle. If $\tan\theta \leq \tan\phi$, the motion downwards is not allowed because the friction exceeds the motive component of weight. This means that even though the motive force is zero, the screw does not move. To ensure the self-locking property, η must be lower then 0.5, in fact if $\eta \leq 0.5 \Rightarrow \tan\theta \leq \tan\phi$.

A second approach to ensure the screw is working properly, i.e. it does not unscrew itself when the wire is pulled down, is here presented. The condition to be imposed is that the friction must be greater then F_{screw} situated in the sloping plane, see Figure 3.14.

$$F_{friction} = F_{normal} * \mu = F_{screw} * \mu * \cos\theta \geq F_{screw} * \sin\theta \Rightarrow \mu \geq \tan\theta$$

Results presented in Chapter 4 show that the device is self-locking.

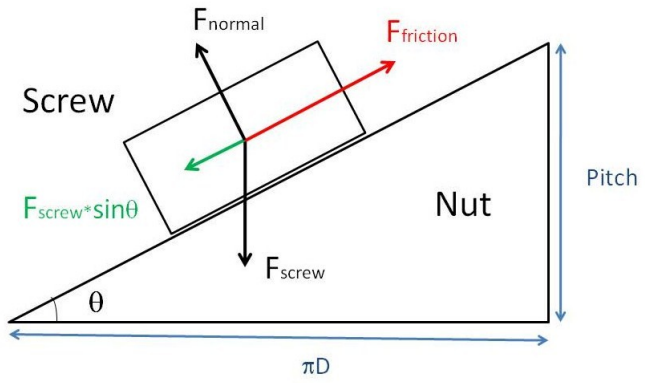

Figure 3.14: Overview of the nut and the screw when the imaginary block is moving downwards.

3.2 Simulations

SolidWorks offers the possibility to set up a virtual real-world environment to test the model design. Simulations can be run to evaluate the performance of the buoy and make decisions to improve the small-scale model.

First of all, the resistance of the lower bearing is analyzed, in order to be sure this component won't break or stop working properly when subjected to the maximum load. The bearing type that has been chosen for the device is a *single row deep groove ball bearing*, the most widely used. It is simple in design, non-separable, suitable for high and even very high speeds and it is robust in operation, requiring little maintenance. Deep raceway grooves and the close conformity between the raceway grooves and the balls enable deep groove ball bearings to accommodate axial loads in both directions, in addition to radial loads, even at high speeds. The lower bearing, placed above the nut, has to endure the weight of the components listed in Table 3.8, whose resulting force is equal to 1.6 N. The worst case scenario occurs when the water level increases of 2 cm: the device must hold an additional force of 9.3 N due to the Archimedes' force, see Table 3.2. The total force the bearing

Component	Weight $[g]$
Screw	100
Piston	20
Upper bearing	7.5
Nut + worm wheel	34
Sum	161.5

Table 3.8: The lower bearing has to endure the weight of the listed components.

has to endure is 10.9 N, for this reason many static simulations have been run applying 11 N on the inner ring subjected to this load, see Figure 3.15 and 3.16. In this particular case, the buoy is not subjected to dynamic loads: in presence of waves the maximum force would be much higher. Figure 3.15 shows a maximum displacement on Ball A, the ball placed where the support is not present.

The ball at its opposite side, Ball B, is the less affected, as one might guess.

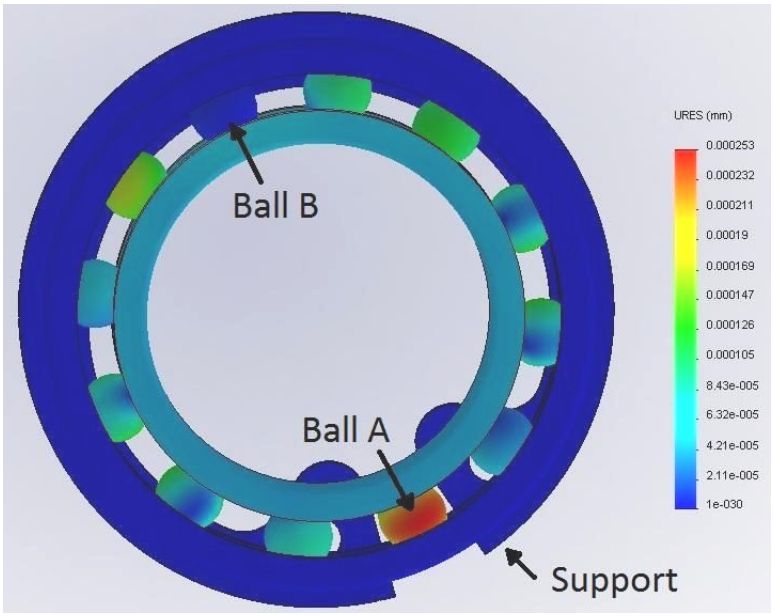

Figure 3.15: Displacement of the lower bearing when loaded by 11 N.

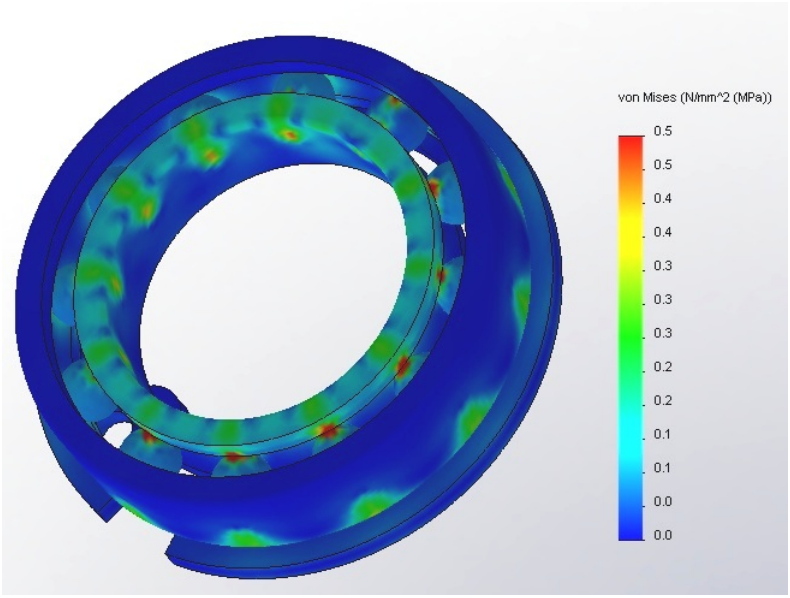

Figure 3.16: Stress on the lower bearing when loaded with 11 N.

However, the maximum displacement registered is 0.0002 mm, a negligible value that can't determine a malfunction of the bearing. The plot displayed in Figure 3.16 shows a stress concentration at the contact points between balls and rings with a maximum value of 3.4 MPa. The tensile strength of this steel bearing is around 400 MPa, hence the maximum stress is faraway from the limit.

A second set of simulations is run on the plastic housing, subjected to a variable load, whose effect must be analyzed. The housing contains the device, the motor and three elements used to balance the total weight, in order to avoid the tilting of the buoy (Figure 3.17 shows the distribution of these elements). The resulting asymmetric load on the base induces displacements and stresses

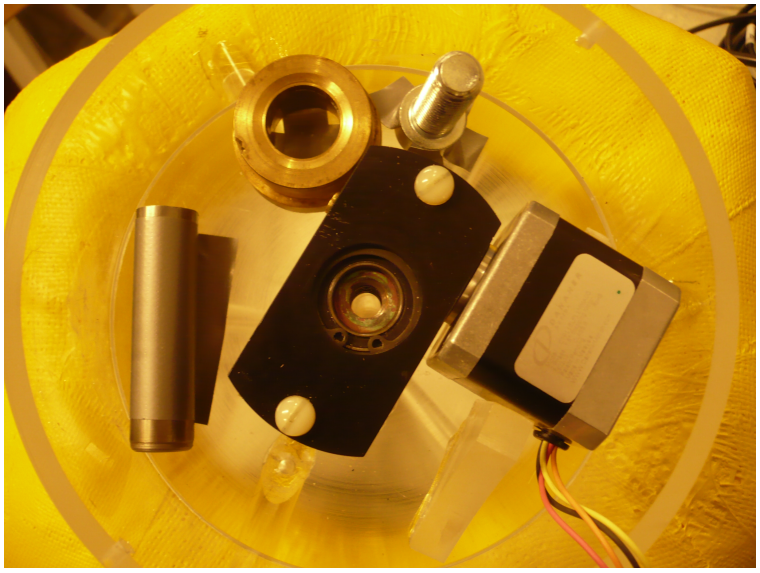

Figure 3.17: Components contained inside the plastic housing.

presented in Figures 3.18 and 3.19. With reference to Figure 3.18, the base is charged with a total load of 18 N distributed as follows:

- 12 N on the device;
- 3 N on the motor;
- 1.5 N on Ele 1;
- 1 N on Ele 2;

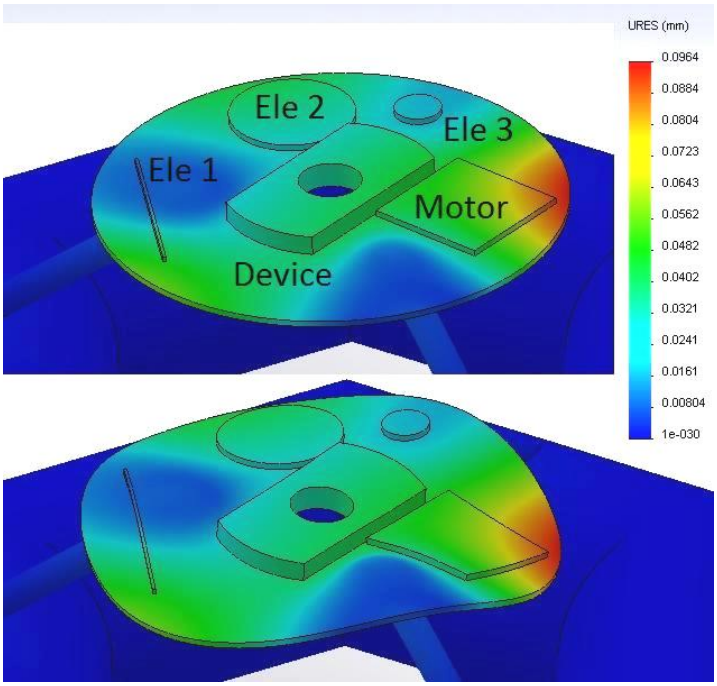

Figure 3.18: The upper picture shows the displacement of the plastic base due to the asymmetrical load of the device, the motor and balancing elements. The lower picture exaggerates the displacement, but it helps to interpret the results.

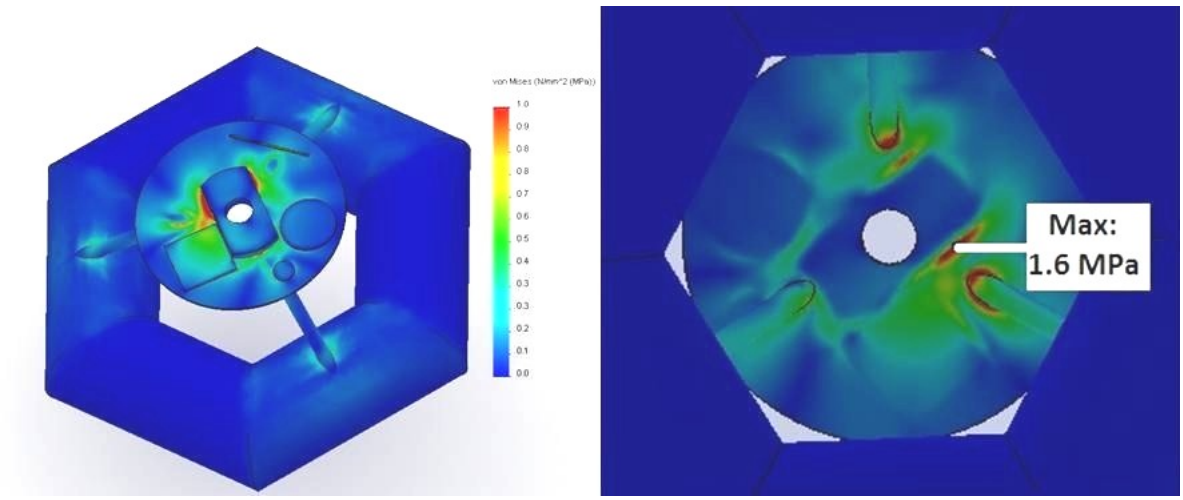

Figure 3.19: Simulations display the stress plot. The picture on the left shows a view from the top of the model, while the one on the right shows a view from the bottom.

- 0.5 N on Ele 3.

SolidWorks calculates a maximum displacement of barely 0.09 mm and a maximum stress of 1.6 MPa. The tensile strength for plexiglass is around 65 MPa, that exceeds the maximum stress registered.

3.3 Motion Control

For the purpose of transforming electrical energy into mechanical energy, the National Instruments Stepper Motion System [20] has been chosen. The essential components of a motion control system (see Figure 3.20) are:

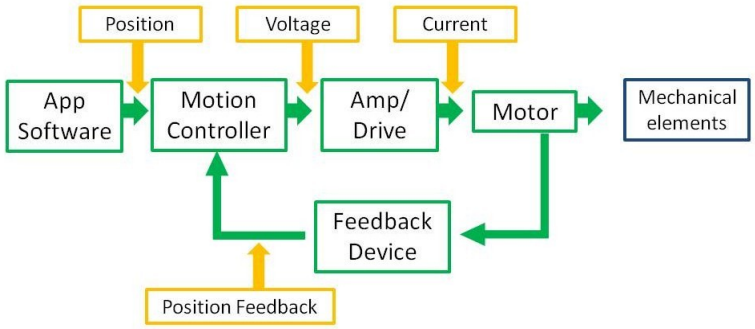

Figure 3.20: Components of a Motion Control System.

- application software, used to command target positions and motion control profiles;
- motion controller, that takes the desired target positions and motion profiles and creates the trajectories for the motors to follow;
- amplifier, which takes the commands from the controller and generate the current required to drive or turn the motor;
- motor, that produces the torque required to move toward the desired target position;
- mechanical element or the device to which the torque is provided;

- feedback device or position sensor, which senses the motor position and reports the result to the controller, thereby closing the loop to the motion controller.

Sometimes it's not necessary to close this loop. More information will be given in the next section.

3.3.1 Stepper Motion System

The hardware and software components selected to build a complete motion control system are:

(a) motor and drive;

(b) motion controller;

(c) accessories and cables;

(d) software.

Firstly, the right motor and drive combination have to be selected. A **NEMA 17 Stepper Motor** has been chosen, because it provides precise positioning and speed control without the use of feedback sensors. This type of motor is a brushless, synchronous electric motor that converts digital pulses into mechanical shaft rotations (see Figure 3.21). Every revolution of the stepper motor is divided into a discrete number of steps, in this particular case 200 steps per revolution. The stepper motor can only take one step at a time and each step is the same size. Since each pulse causes the motor to rotate a precise angle, typically 1.8°, the motor's position can be controlled without any feedback mechanism, because the rotation angle of the motor is proportional to the input pulse. The possibility to have an open-loop control makes the motor simpler and less costly to control. Precise positioning and repeatability of movement are guaranteed since a good stepper motor have an accuracy from 3 to 5% of a step and this error is non-cumulative from one step to the next.

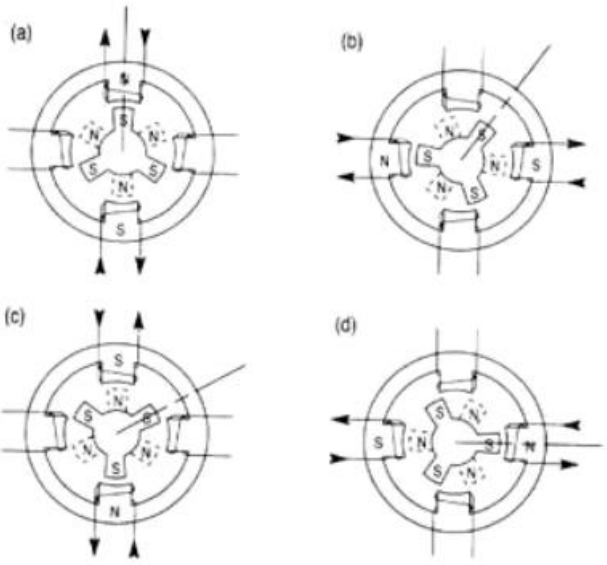

Figure 3.21: Movement of the stepper motor rotor as current is pulsed to the stator. (a) Current is applied to the top and bottom windings, so the top winding is north, (b) Current is applied to left and right windings, so the left winding is north, (c) Current is applied to the top and bottom windings, so the bottom winding is north, (d) Current is applied to the left and right windings so the right winding is north. (Credits to NI)

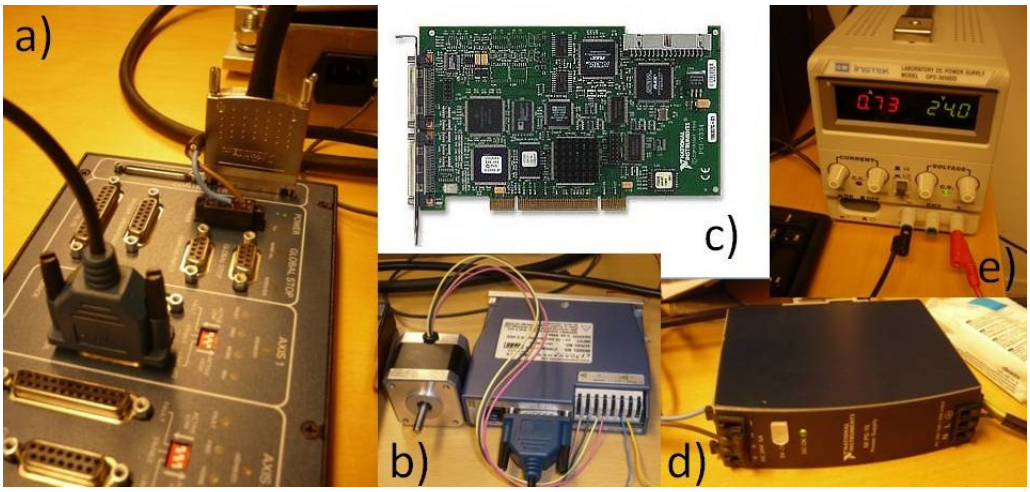

Figure 3.22: Hardware components of the Stepper Motion Control System. a) UMI, b) motor and driver, c) motion controller, d) UMI's power supply, e) driver's power supply.

The drive that better fits with the NEMA 17 Stepper Motor is the **NI Stepper Drive P70530**, shown in Figure 3.22b. It requires a power supply (Figure 3.22e), that must provide an output voltage between 20 and 75 VDC.

Secondly, the **NI 7332 Low Cost Stepper Controller** has been chosen, see Figure 3.22c. The motion controller acts as the brain of the motion control system and calculates each commanded move trajectory.

The third step is to select the accessories, like the **NI UMI 7772** interface and cables, see Figure 3.22a. The single cable **SHC68-C68-S** from the motion controller to the UMI carries input and output signals. The UMI interface simplifies integration of drivers, amplifiers, encoders, limits, and I/O with NI controllers, using a 24 VDC power supply (Figure 3.22d).

Lastly, the software **LabVIEW 2010** is selected to prototype the motion application and convert the project into a ready-to-run code. The code implemented is described below, showing both the front panel and the block diagram.

3.3.2 Front Panel

The front panel is divided in two parts for the purpose of building a simple and intuitive interface between the user and the motor, see Figure 3.23.

The left side of the front panel contains the parameters which have to be set:

- Axis Number to be used and Board ID that corresponds to the Motion Controller in the Board Configuration Utility;
- Velocity, Acceleration and Deceleration of the motor and Frequency of the Control;
- Enable Set Water Level. The default value of the initial water level is zero, so that it is possible to change this setting by using the boolean switch Enable Set Water Level. If an experiment ends with a final water level different from zero and a new test would be carried out, it won't be necessary to fill in or empty the tank to reach 0 cm. Moreover, the screw will change automatically the position of its center in agreement with the initial water level set.

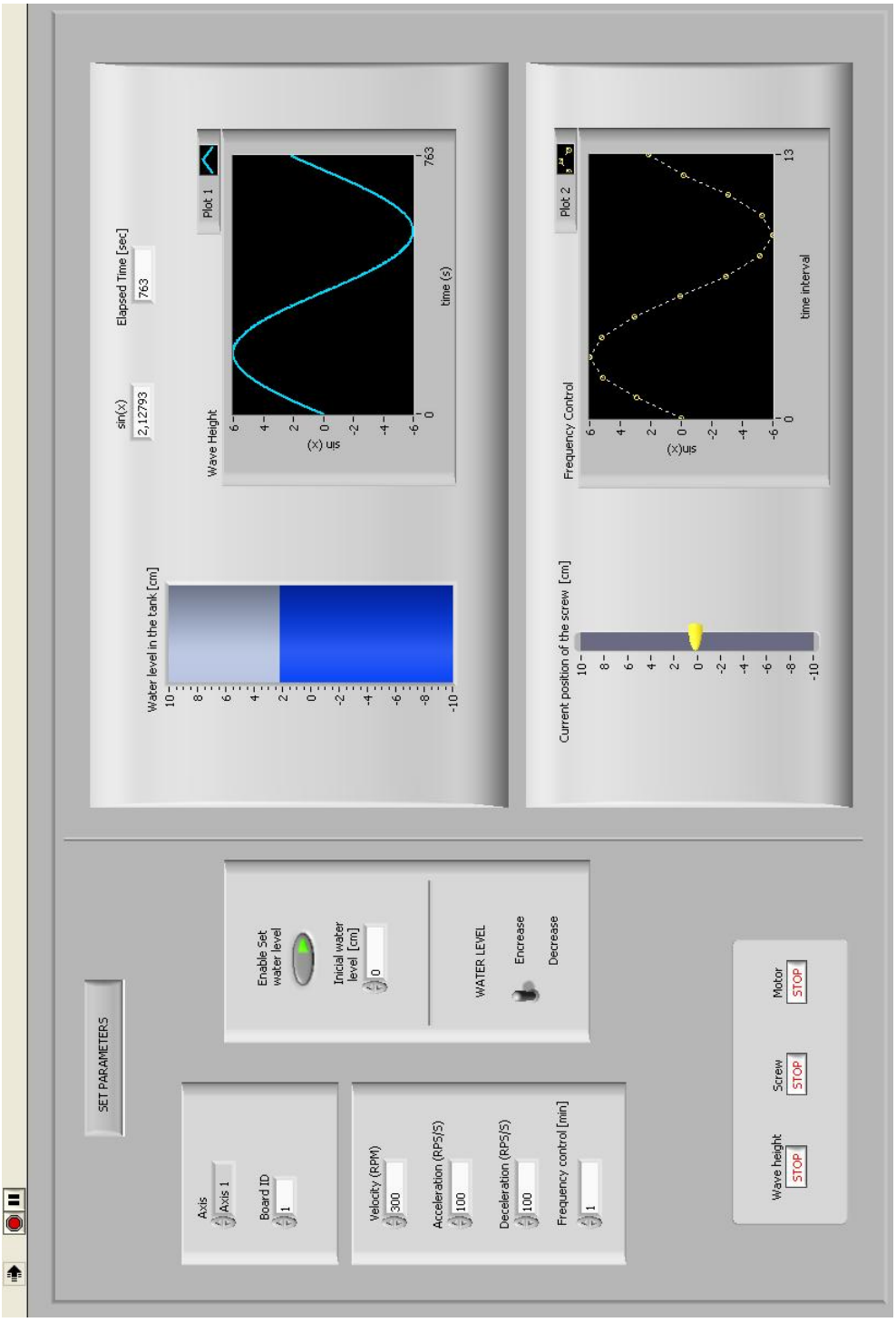

Figure 3.23: Front panel of the LabVIEW program.

- Level Increase/Decrease. The program starts raising the water level by default, but this switch allows to reverse the direction of the level's variation.

Once all parameters are been set, the program can run. The results are shown in real time within the right side of the front panel. In the upper area a numeric indicator and a chart display the variation of water level in the tank. The variation follows a sinusoidal profile in order to simulate a real tide. The amplitude and the frequency of the sine function are calibrated so that tides turn out to be ± 1 m high and the complete tide's cycle lasts 12 minutes. Every minute corresponds approximately to one hour in the real world. In the lower area the position of the screw's middle point and the frequency chart are displayed. In the example shown in Figure 3.23, each minute the program reads the measurement of the water level and stars up the motor, that has to reach the new position and wait for the next command. The same example shows that the amplitude of the sine function is only 6 cm: it is possible to change the hight of the tidal wave as desired within the code, hence the program is suitable for different case studies.

3.3.3 Block Diagram

The block diagram, shown in Figure 3.24 is divided in three frames and contains seventeen sub-VIs. The part of code written in each frame executes sequentially, from left to right. This structure, called Flat Sequence, ensures that a subdiagram executes before or after another subdiagram. The data leaves each frame as the frame finishes executing, thus the input of one frame can depend on the output of another frame.

In the first subdiagram, two .tdms files are created for the purpose of saving the data which will be produced in the second frame. Inside the last frame the .tdms files are opened and the file data is presented in the TDMS File Viewer dialog box. The measurements can be easily imported in Excel if additional calculations or analysis of the data are required. Going back to the

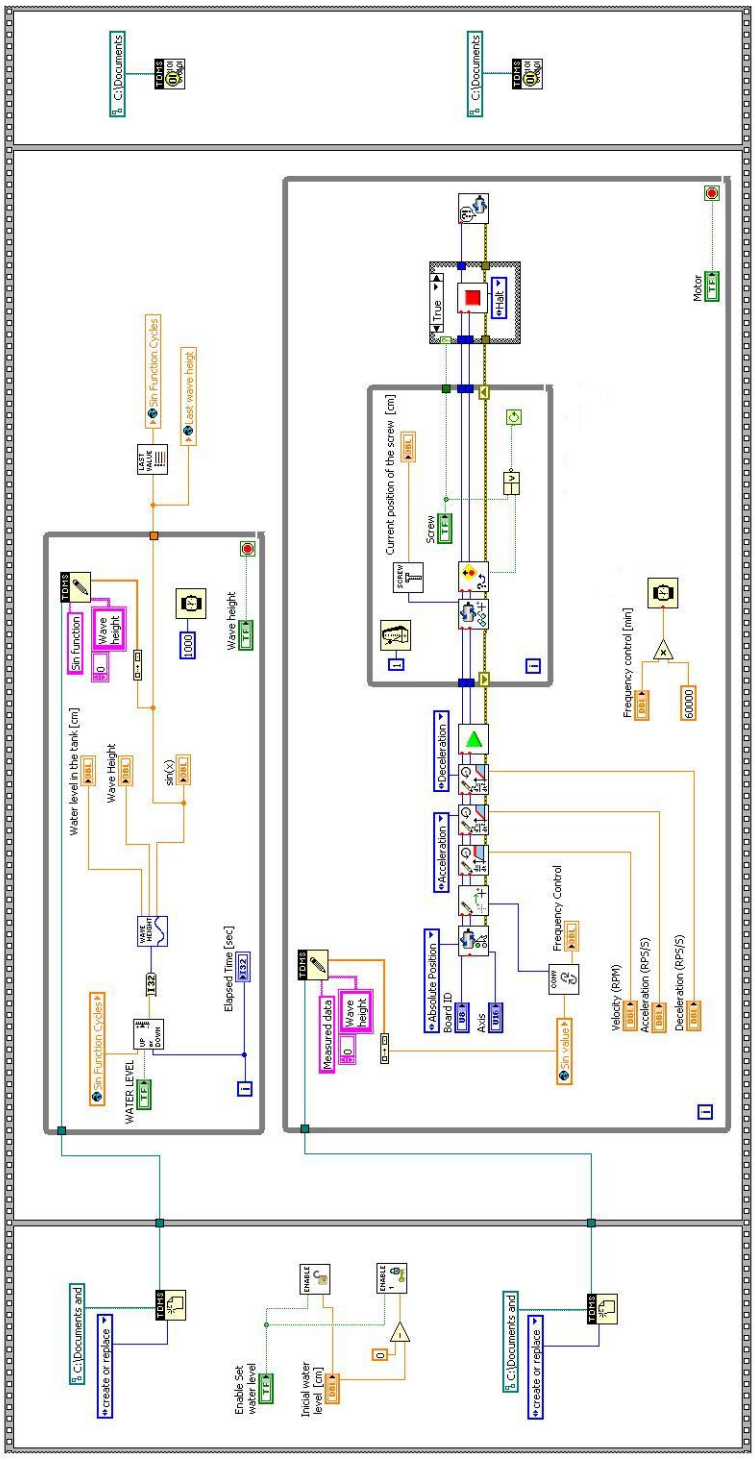

Figure 3.24: Block diagram divided in three frames with seventeen sub-VI.

first subdiagram, the two sub-VIs ENABLE and ENABLE 1 permit to set the value of the initial water level and the position of the screw, see Figure 3.25 and 3.26. ENABLE 1 contains another sub-VI, ADJUST, that allows to adjust the central position of the screw if desired. In the second frame, there are

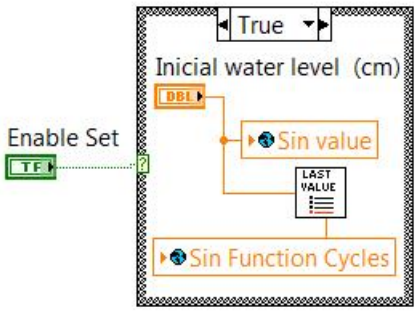

Figure 3.25: Sub-VI ENABLE.

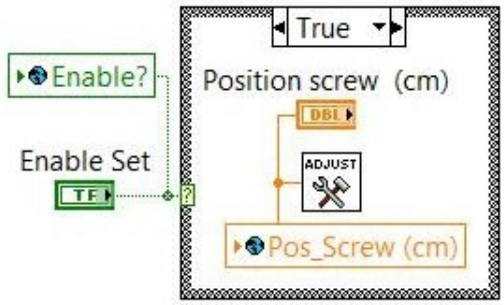

Figure 3.26: Sub-VI ENABLE 1.

two While Loop which run simultaneously. The upper one generates the sine function that simulates tides. This part of the code uses three sub-VIs: UP or DOWN, to choose the direction of the water level variation, see Figure 3.27; WAVE HEIGHT, to display the sine function and calibrate its amplitude and frequency, see Figure 3.28; LAST VALUE, to memorize the number of cycles the While Loop made, in order to start the next experiment from that value, without going back to zero by default, see Figure 3.29.

The lower While Loop contains the Simple One-Axis Move VI (Figure 3.30), that completes a move to a user-specified position on a single axis. Inside this

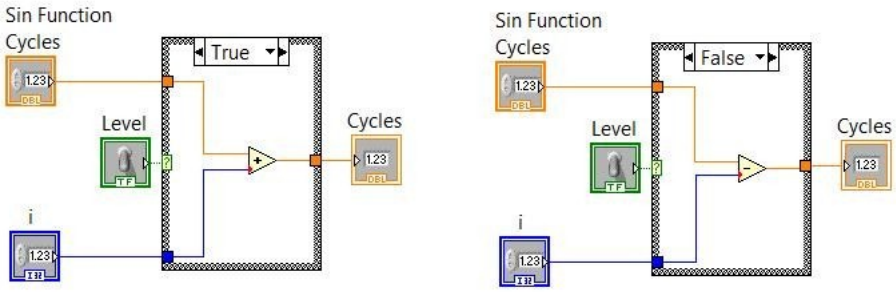

Figure 3.27: Sub-VI UP or DOWN.

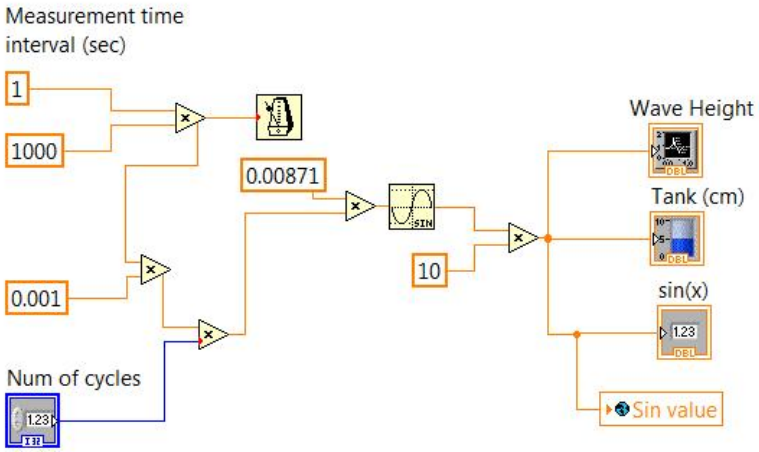

Figure 3.28: Sub VI WAVE HEIGHT.

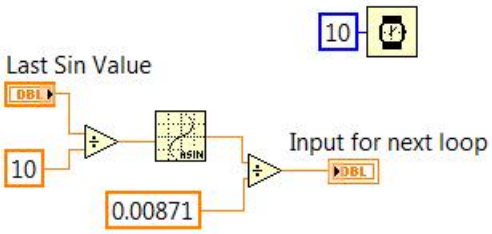

Figure 3.29: Sub-VI LAST VALUE.

loop there is another While Loop which monitors the position of the screw. The

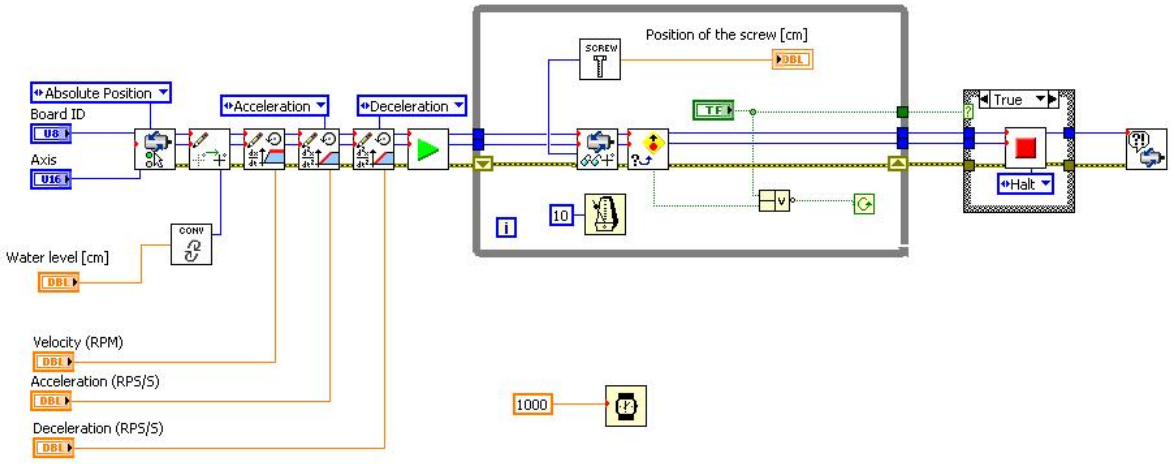

Figure 3.30: Simple One-Axis Move VI.

current position indicator is continuously updated until the Move Complete Status for the specified axis is TRUE. In the lower loop there are two sub-VIs, called CONV and SCREW, see Figure 3.31: the first converts the water hight from *cm* to *steps* and the second vice versa. These VIs take into account that the motor makes 200 steps per revolution and that 20 revolutions of the motor's shaft correspond to one complete rotation of the nut, that is 3 mm of displacement of the screw.

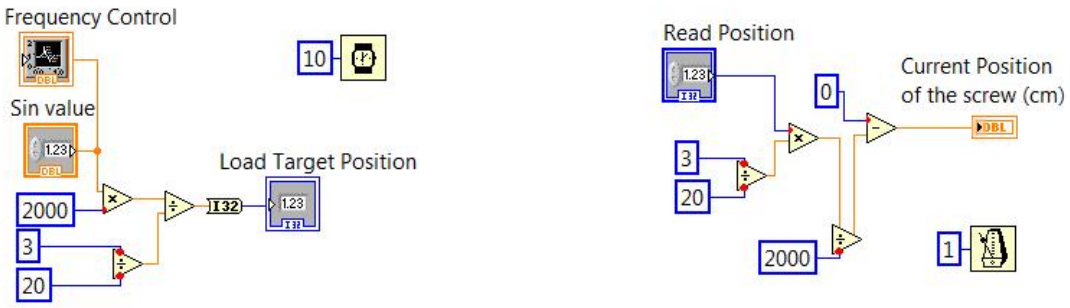

Figure 3.31: Sub-VIs CONV on the left and SCREW on the right.

3.4 Laboratory experiments

3.4.1 Simulation of tide

Small scale buoys are usually tested in a tank placed in the workshop of the Division for Electricity. This tank is 1.2 m high, 4 m long, 1 m wide approximately, and it is provided with a wave generator, mounted on the right side, and a wave absorber, located on the left side, see Figure 3.32.

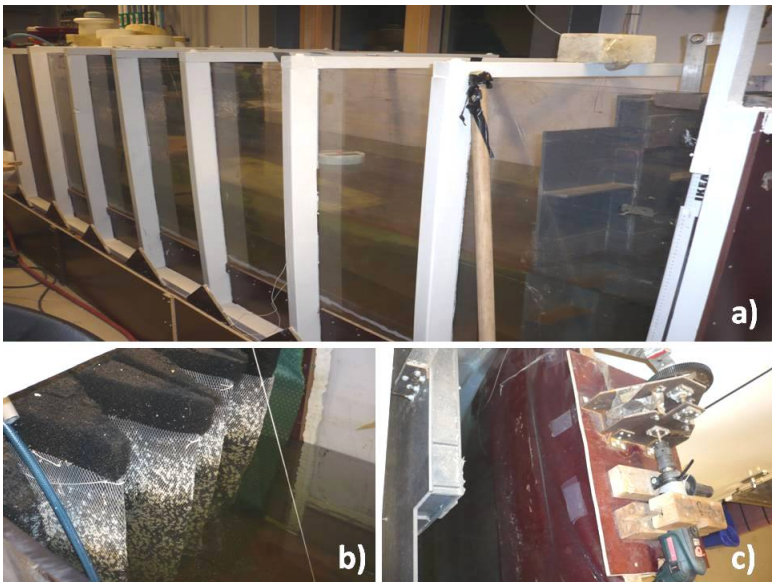

Figure 3.32: Picture a) shows the tank where the buoy is tested, while b) is a wave absorber placed on the opposite side of the wave generator, c).

In order to simulate tides, the water level is increased by filling the tank through a tube connected to a tap and decreased by emptying it using a pump. The Wolfcraft Pump used to reduce the water level is small and compact, and it is attached to a power drill, as shown in Figure 3.33.

Furthermore, it has flanges at the base, so that it can be permanently mounted on a board. The specifications of the pump are summarized in Table 3.9.

This simple way of changing the level does not permit an exact reproduction of the sine function which characterizes a tidal wave. The variation of the level is constant when the tank is filled in: the level increases of 1 cm every minute on average. The variation is constant even using the pump, but with

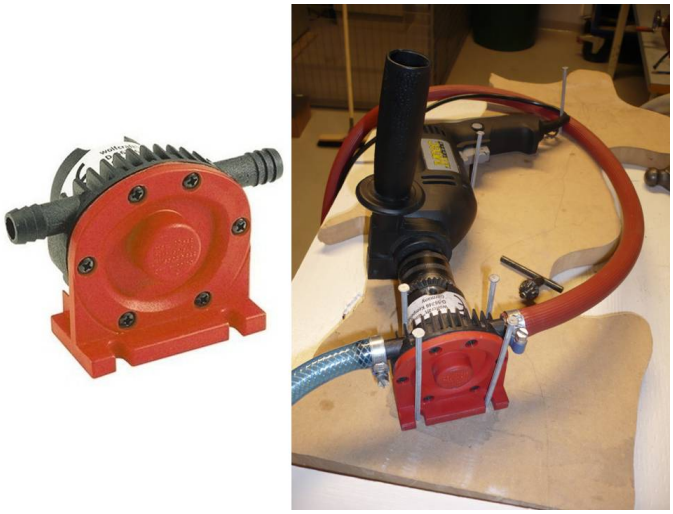

Figure 3.33: Wolfcraft Pump used to change the level of water in the tank.

Throughout [liters per hour]	1300
Max priming hight [m]	15
Dry running limit [sec]	30
Weight [grams]	9.1

Table 3.9: Pump's specifications.

a different ratio: the level decreases by 1 cm during six minutes.

3.4.2 Program in LabVIEW

For the reason just explained, the LabVIEW program previously described (see the section regarding Motion Control) can not be used to control the motor in such conditions. Two possible solutions are:

- to measure the water level every fixed interval of time and send the signal to the motor,
- to choose a determined variation of the level and to move the screw by the same variation regardless to time.

The tank is not provided with a sensor of water level, so that an expeditious solution is adopted, i.e. reading manually the water level from a measuring tape. The second approach listed above appears to be the best one, because it is easier to read an integer on the tape, then a decimal after a fix interval of

time. For this purpose another program is generated in LabVIEW: it permits setting the water level without taking into account the elapsed time. In the left area of the front panel the velocity, acceleration and deceleration, the water level can be set, while the position of the screw is displayed on the right, see Figure 3.34.

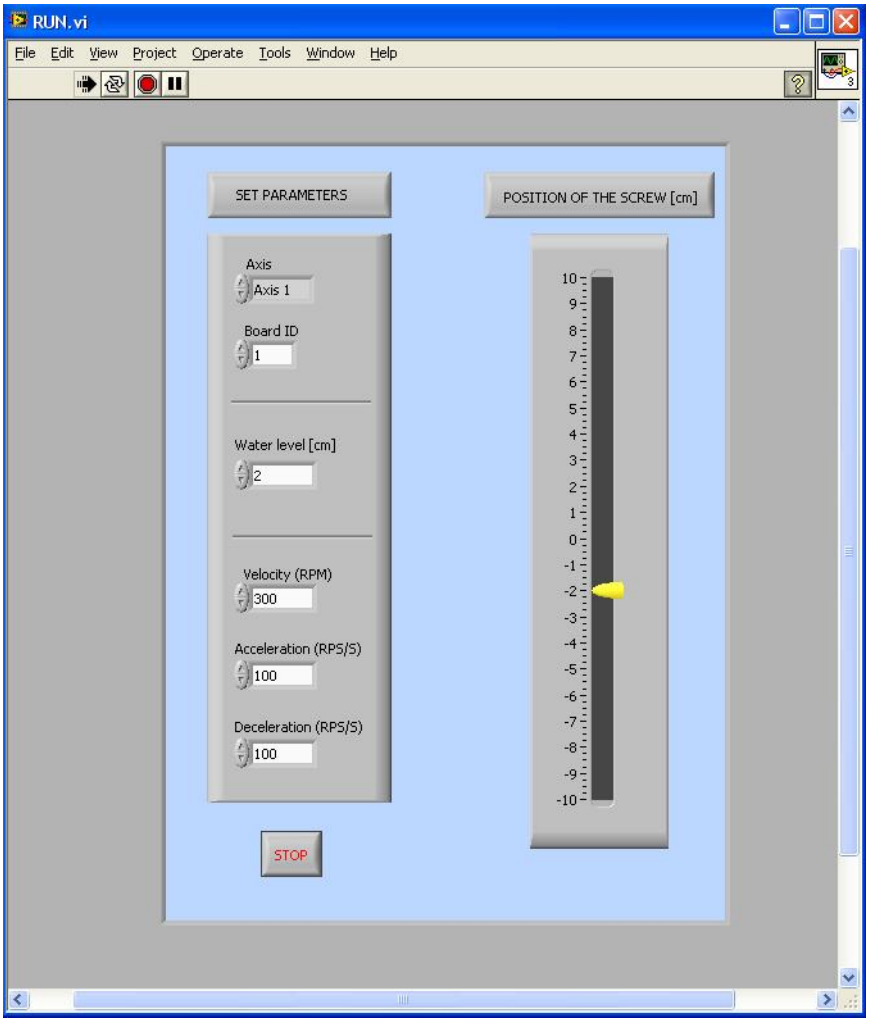

Figure 3.34: Front panel of the program used to test the model in the tank.

The block diagram is a Simple One-Axis Move VI, similar to the one implemented in the first program, see Figure 3.30.

3.4.3 Small scale generator

A small generator was built, in order to evaluate the voltage production with and without the adjustment of the wire. The generator consists of two elements listed below.

(a) A wood and steel structure which contains a pulley. The wire connected to the buoy goes inside the structure, rolls along the pulley and goes outside to reach a motor. A stick is attached to the wire (see Figure 3.35) and it simulates the translator that moves inside the stator.

(b) A DC motor placed above the water level. The wire revolves around its shaft and transfers the vertical motion of the buoy to the motor.

In presence of simulated high tides the translator beats the upper part of the structure; on the contrary, the translator's motion is bounded to the lower part of the structure during simulated low tides. The voltage is recorded by an oscilloscope connected to the motor. In the next chapter results obtained by using the small scale generator are presented with the purpose of showing the difference in voltage production for many water levels and wave heights.

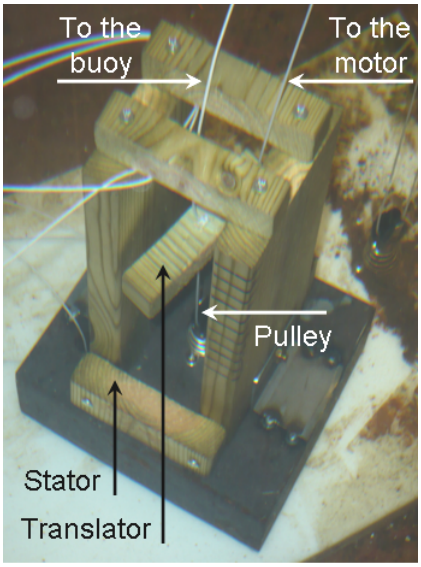

Figure 3.35: The small scale generator placed in the bottom of the tank. The structure is made of wood and steel, and every centimeter of the lateral side is marked.

Chapter 4

Results and discussion

The aim of the current chapter is to discuss the results given in the previous chapter, although some comments have already been made.

Motor's torque

The motor has to supply a torque between 0.0002 and 0.0003 Nm to move the screw, as shown in Table 3.7. In order to demonstrate that the motor is able to provide such a torque, some calculations are made and the result is presented below.

The current, I, and the voltage, V, that reach the motor during the motion are observed on the two-dimensional graph of Figure 4.1. Both signals can be simplified as sine functions, having different amplitude and phase. In order to calculate the real power, the average value of the instantaneous active power is introduced:

$$P = V_{RMS} I_{RMS} \cos\theta$$

where:

$$V_{RMS} = \frac{2.5}{\sqrt{2}} = 1.77V$$

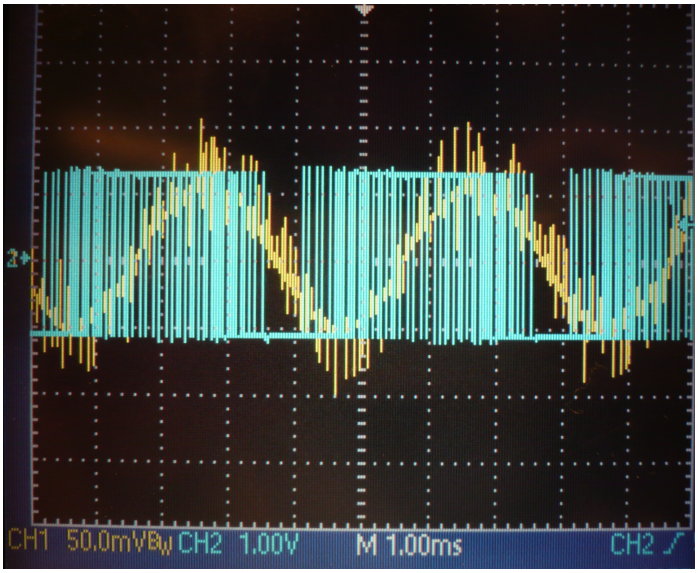

Figure 4.1: The oscilloscope shows the current in yellow and the voltage in blue during the motion.

$$I_{RMS} = \frac{0.5}{\sqrt{2}} = 0.35A$$

$$\theta = 72°$$

with θ being the phase difference between V and I.

The power delivered by the motor's driver to one winding is $P = 0.19W$. The stepper motor has got two windings, for this reason the total power delivered doubles: $P = 0.38W$. If the speed is set to $v = 300RPM$, the resulting torque, M_m, is expressed by:

$$M_m = \frac{60 * P}{2\pi * v} = \frac{60 * 0.38}{2\pi * 300} = 0.012Nm$$

Being $M_m > M_s$, the motor is able to move the screw. The difference between the two values of torque calculated is due to the fact that:

- the efficiency in the conversion from electrical power to mechanical power was not considered,
- the real value of the friction coefficient is unknown and the ones used

before could reveal themselves underestimated,

- more power is required when a misalignment of the screw occurs and tests made on the model show that is happens.

However, values of M_m and M_s differ by two order of magnitude, it suggests that the motor has a low efficiency or it is oversized. According to the National Instrument Technical Support the efficiency of the NEMA 17 has never been tested, but many statements say that the motor is not efficient.

On the other hand, the motor is enough powerful to push the buoy under the water surface (see Figure 4.2) overcoming the Archimedes' force and holding the screw in position. Holding the buoy down the water level can be useful to

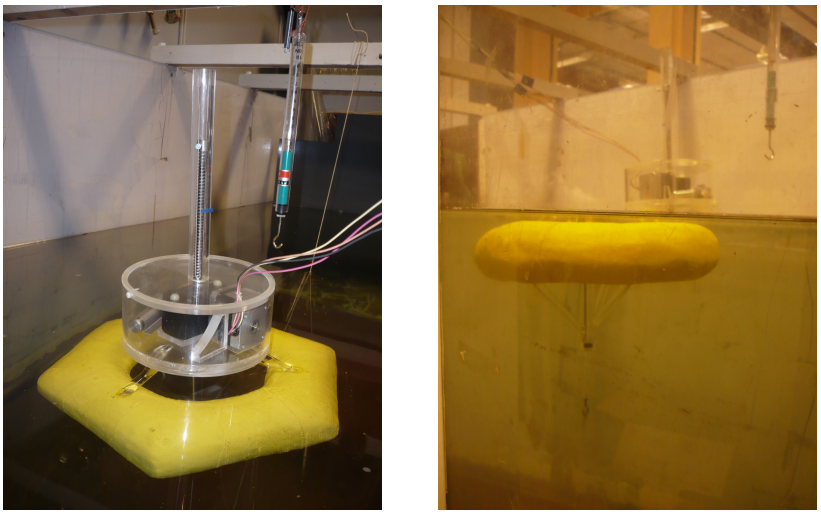

Figure 4.2: The motor is able to hold the buoy under the water.

reduce the volume exposed to severe weather, e.g. when a storm occurs or the water freezes. The value M_s is recalculated considering the additional force of 12 N (see Table 3.7) and the resulting torque is presented in Table 4.1.

	μ_1	μ_2
M_s [Nm]	0.002	0.003

Table 4.1: Values of torque necessary to hold the buoy under the water level for different friction coefficients.

Buoyancy

Figure 3.10 showed how the immersed volume of the buoy looks like when the water level increases. The wire is subjected to the force F_{wire} that changes as presented in Table 3.2. According to these values, the red line in Figure 4.3 has been drawn.

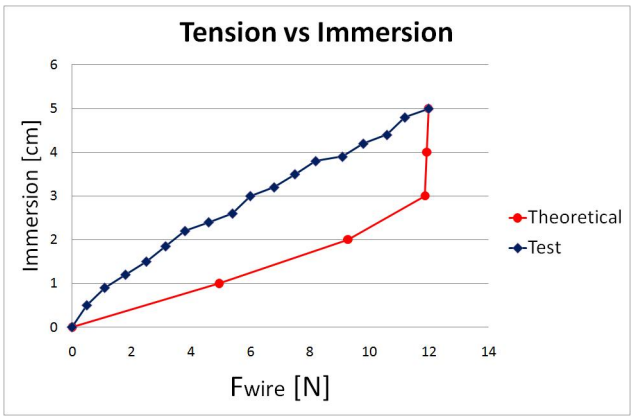

Figure 4.3: Comparison between theoretical and experimental curves.

The theoretical line indicates that F_{wire} is equal to 12 N approximately when buoy is totally submerged, while the last two values correspond to the immersion of the pipes, whose volumes are small, so that the result is a negligible variation of tension. A test is carried on in the tank to investigate if the real behavior of the model is well described by the theoretical one. The dark blue line in Figure 4.3 represents the tension in the wire for different values of immersion of the model. A dynamometer is used to register this variation, as shown in Figure 4.4. The dynamometer is attached to the wire that goes around a pulley, fixed on the bottom of the tank, to reach the piston's hook. The blue curve (Figure 4.3) does not coincide with the red one because of the pulley's friction, whose effect is to soften up the experimental curve, and because the shape, hence the volume, of the model is not exactly equal to the one drawn in SolidWorks. However, the final result for both the theoretical and the experimental curve is that the tension gets up to 12 N when the buoy is completely submerged.

For the purpose of investigating the behavior of the model in presence of waves,

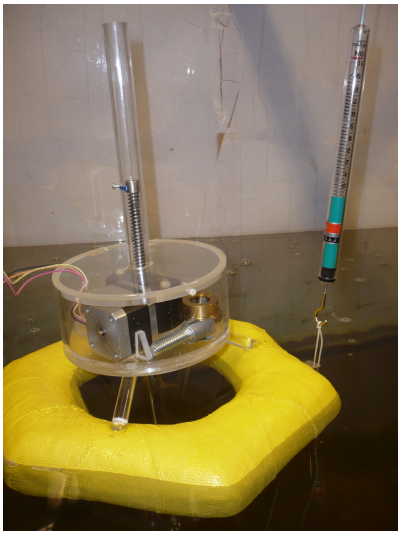

Figure 4.4: Dynamometer used to calculate the tension in the wire when the water level increases. The wire attached to the piston goes around a pulley fixed on the bottom of the tank and then goes up to reach the dynamometer.

the generator of waves is activated. A dynamometer is hooked to the wire and the tension accumulated is registered. Waves 5 cm high are generated and a variation of 1.5 N is read on the dynamometer. Even this time, the unscrewing is not expected and the motor works properly.

Self-locking property

One of the reason why the device described in Figure 3.5 has been chosen is that it has the property to be self-locking. No matter what the force acting on the screw is, it keeps its position without unscrewing. To verify that the device is self-locking, the efficiency of the inclined plane for both the nut and the worm (Figures 3.11 and 3.12) has been calculated. The values of efficiency calculated for different friction coefficients ($\mu_1 = 0.15$ and $\mu_2 = 0.25$), are shown in Table 4.2. They satisfy the condition $\eta \leq 0.5$, so that the device is demonstrated to be self-locking.

	μ_1	μ_2
η_{screw}	0.44	0.32
η_{worm}	0.39	0.28

Table 4.2: Efficiency of the inclined planes.

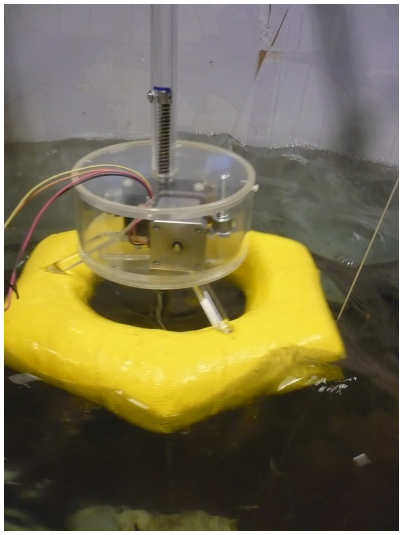

Figure 4.5: The model is tested in presence of waves produced by the wave generator placed in the tank.

The second approach to ensure the screw does not unscrew itself when the wire is pulled down was described in Section 3.1.2. As expected, $\tan\theta$ results lower then μ for both screw and worm wheel, see Table 4.3.

$\tan\theta_{screw}$	0.12
$\tan\theta_{worm}$	0.10

Table 4.3: $\tan\theta_{screw}$ and $\tan\theta_{worm}$ are lower then the friction coefficients μ_1 and μ_2.

SolidWorks Simulations

To decide if the SolidWorks simulations pass or fail some criteria have to be established, for example, understanding the mechanism of potential failure leads to the evaluation of stress results. The first static simulation regarding the bearing shows that the maximum stress is located on the contact points between balls and inner ring (Figure 3.16). This is reasonable because the external force is located on the top of the inner ring, so that a potential failure can be expected in that region. The Von Mises stress measure is used in the simulation to evaluate the structural safety of the bearing. This method is

widely utilized to describe the stress acting on elastoplastic materials, like steel. For this reason, it has been chosen to carry out this analysis. The second static simulation gives an idea about the behavior of the housing that contains the device and the motor. The plastic housing is subjected to the different weights of asymmetrical components and it is supported by three pipes symmetrically ordered. Results show that the displacement increases in areas where the weight is high and the support is absent (see Figure 3.18). Conversely, the stress increase in the region where the weight is high and the pipe is present (see Figure 3.19), so that these plots seem to be reasonable too. Values of maximum displacement and stress for both simulations don't exceed the limits, hence the model neither will not break nor malfunction. For more detailed information see Section 3.2. However, the simulations performed in SolidWorks are static ones, so that results obtained are referred to the interval of time in which the motor is not working. More advanced simulations could be carried out using other tools that SolidWorks offers.

Motion Control

The LabVIEW program described in the Section 3.3 is appreciable from the theoretical point of view and very easy to use. Although it is true, a technical limitation precludes its utilization: during tides, the water level changes according to a sine function, which was not possible to reproduce in the tank where tests were carried out. The solution adopted is to choose a determined variation of the level and to move the screw of the same variation regardless to time. For this reason, a second program has been written: it allows to set the water level without taking into account the elapsed time, see Figure 3.34. In this case, the motor's motion is not completely automatic, requiring someone who reads the level from a measuring tape and starts the program every time a new level is reached. A level sensor would be useful, so that the sensor itself can directly give the signal to the motor. For example, an MT Profil Water Level Gauge can be mounted on the tank, see Figure 4.6. It is a mechanical float operated, tank contents gauge, universally adjustable, with

Figure 4.6: MT Profil tank contents gauge.

interchangeable scale 0-150 or 0-250 cm, and it costs around 100 SEK. This is one of the cheapest solutions, but some more professional tools are available, like optical or ultrasound sensors.

Control Frequency

The first LabVIEW program, described in the Section 3.3, allows to set the frequency of the control. The full scale generator's efficiency decreases when the water level deviates of 25 cm, that corresponds to 2.5 cm of variation in the tank. For this reason, a suitable time interval has to be chosen, so that the motor starts before a level's change of 2.5 cm is registered. For safety, this level's variation is reduced to 2 cm. Figure 4.7 shows the result of different tests obtained by changing the control frequency. The interval time of 20 seconds has proved to be the most appropriate. As the figure shows, the number of controls seems to be too much dense next to high and low tide peaks. Adjusting the screw after the signal of the water level sensor appears more convenient, so that the motor is activated only when necessary with a frequency that changes during the tide's cycle. In the tank there is not a level sensor and this test can't be made, but it is a useful suggestion for future developments of this project.

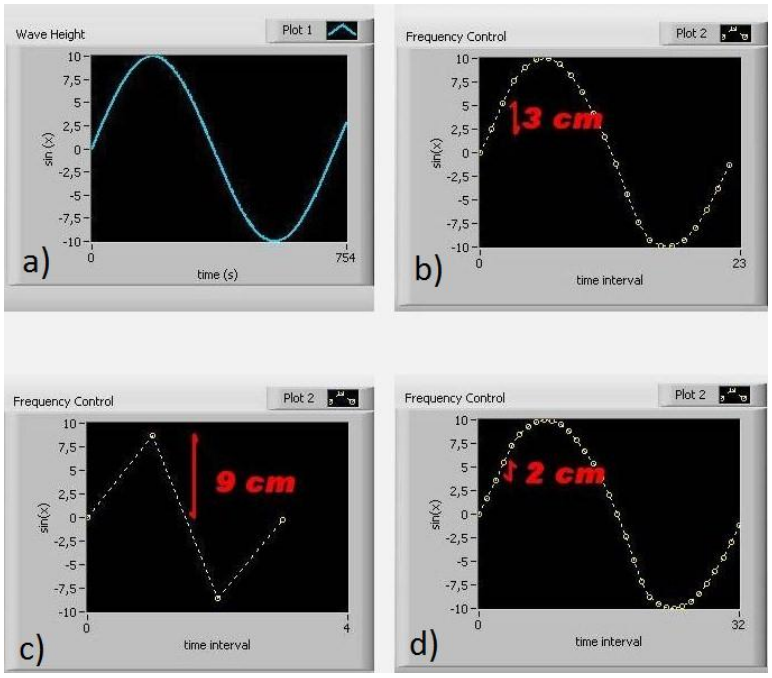

Figure 4.7: The picture (a) shows the variation of water level during a tide, while the other charts represent different tests performed by changing the frequency of the control: (b) 30 seconds, (c) 4 minutes, (d) 20 seconds.

Voltage with and without adjustment

Some tests are carried out to evaluate the difference between the voltage produced using the adjustment device and the one produced without using it.

The first set of tests was realized by running the buoy through a 4 cm wave height. The maximum voltage recorded is 1.2 V when the relative water level is zero. By adjusting the length of the wire, this value remains constant when the water level increases and decreases, but the voltage changes if the device is not activated, as Figure 4.8 shows. In this chart, indicators represent the peaks of voltage for increasing water levels. A tendency line is added to the graph, in order to see what the trend is. The curve shows that the voltage produced when the water level decrease is lower that the one produced when the level increase; for example, if the level is -8 cm, the peak voltage is 0.2 V, but if the level goes to +8 cm, the voltage is 0.9 V (see Table 4.8).

The second and third sets of tests were carried out to verify the same tendency or deny it. The second set is characterized by a wave height of 6 cm, and the

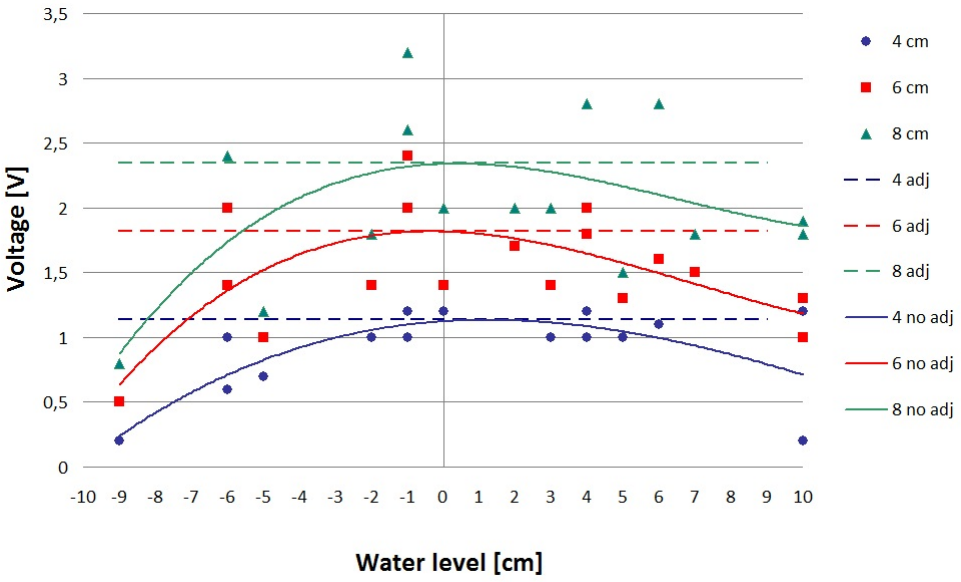

Figure 4.8: Experimental results of the voltage recorded for different wave heights and water levels.

waves of the last set are 8 cm high. Both sets confirm that the production of energy, proportional to the voltage, is lower during simulated low tides, as shown in Figure 4.8. As before, the voltage is constant if the device is activated, because the translator completes a full stroke for each wave. With reference to Figure 4.8, the voltage function is a concave curve in absence of adjustment system, but this function can be considered as an horizontal line when the device is in action. The linear equation intersect the curve in its peak, so that it is possible to write the following three equations referred to each wave heigth (a):

- $y = 1.2$ if $a = 4$ cm,
- $y = 1.8$ if $a = 6$ cm,
- $y = 2.3$ if $a = 8$ cm.

From the equations of the the tendency lines, a voltage value for each level and wave height is calculated (see Table 4.4). Table 4.5 presents the percentage of produced voltage for every water level, comparing the numerical results of Table 4.4 with the linear function. Looking at Table 4.5, it can be noticed

that the voltage decreases by 16-26% when the water level reaches +8 cm, and decreases by 48-64% when the level goes down to -8 cm. It is very important to view the presented results qualitatively rather than quantitatively. The Reynolds number of the scaled experiment, as well as the elementary experimental setup, limits the veracity of the results. Although they cannot predict real values of energy production, they give a clear qualitative representation of the effect of tides.

		Water level [cm]																
		-8	-7	-6	-5	-4	-3	-2	-1	0	1	2	3	4	5	6	7	8
Wave	8	1.2	1.5	1.7	1.9	2.1	2.2	2.3	2.3	2.3	2.3	2.3	2.3	2.2	2.2	2.1	2.0	2.0
height	6	0.9	1.2	1.4	1.5	1.6	1.7	1.8	1.8	1.8	1.8	1.8	1.7	1.6	1.6	1.5	1.4	1.3
[cm]	4	0.4	0.6	0.7	0.8	0.9	1.0	1.1	1.1	1.2	1.2	1.2	1.1	1.1	1.1	1.0	0.9	0.9

Table 4.4: Numerical results of the produced voltage [V].

		Water level [cm]																
		-8	-7	-6	-5	-4	-3	-2	-1	0	1	2	3	4	5	6	7	8
Wave	8	52	64	74	83	89	94	97	99	100	100	99	98	95	93	90	87	84
height	6	51	64	75	84	90	95	98	100	100	99	97	94	90	86	82	77	72
[cm]	4	36	50	62	72	80	87	93	97	99	100	100	99	96	92	87	81	74

Table 4.5: Produced voltage in percentage for different water levels and wave heights.

Costs

The realization of the model required a certain amount of money. The cost of processing, construction and materials for the device was 12766 SEK, paid to DIONE KULLAGER AB. Secondly, 26473 SEK were paid to National Instruments Sweden AB for the hardware of the Motion Control System. Finally, materials and tools have been bought to build the buoy and make it waterproof for the amount of 1000 SEK approximately. The total cost of the model was about 40000 SEK, which could be lowered by building a different system to control the motor. On one hand, the motion control would have been prized down; on the other hand, a wider knowledge about automation would have been required.

Chapter 5

Conclusion

A scaled model of a system for compensating the tidal effect has been designed and constructed, and experiments have been conduced to verify the concept. The experimental work reported on in this thesis lead to the conclusions listed below.

- The solution adopted to minimize the tidal effect on WECs shows potential for further developments. The device works in a proper way and with very high accuracy (9 μm per revolution of the nut).
- The mechanical system is very simple as dictated by the Lysekil wave power project. The need of maintenance won't be very frequent in a future full scale model. If problems occur, the system components are easy to reach since they are placed above the water level.
- Some analysis are made to dimension the model:
  - the buoyancy has been evaluated in order to ensure that the model does not sink and the sensitive parts will not be immersed during normal operation;
  - the torque the motor has to deliver to move the screw has been calculated for different values of friction coefficients (see Table 5.1) and the results are compared with the real torque the motor provides, 0.012 Nm;

			M_s [Nm]
μ_1	=	0.15	0.0002
μ_2	=	0.25	0.0003

Table 5.1: Values of torque for different friction coefficients.

– a similar analysis has been carried on to demonstrate that the motor is able to hold the buoy under the water level, overcoming the Archimedes' force of 12 N (see Table 5.2);

			M_s [Nm]
μ_1	=	0.15	0.0017
μ_2	=	0.25	0.0033

Table 5.2: Values of the torque, when the buoy is under the water level.

– to verify that the device is self-locking, the efficiency of the inclined plane was evaluated both for the nut and the worm, proving that $\eta < 0.5$ in both cases;

- Simulations have been run in SolidWorks to examine the behavior of the bearing and the plastic housing when subjected to the load due to the weight force and the Archimedes' force. The result is that in both cases the possibility of breakage or malfunction is remote (see Table 5.3).

	Max Displacement [mm]	Max Stress [MPa]
Bearing	0.0002	3.4
Housing	0.09	1.6

Table 5.3: Maximum values of displacement and stress calculated by SolidWorks Simulation.

- The energy production seems to be lower during low tides rather than during high tides, and the use of an adjustment system brings the production to the maximum.

- The environmental impact does not change because neither oil nor grease is used to lubricate the screw and the nut. From the visual impact point of view, a new element is visible beside the classic point absorber. The upper pipe containing the screw can be used to place a positioning light

on the top of it to localize the buoy during the night and in case of severe weather. Furthermore, the scaled buoy is twenty times smaller than the real floater, while the device is only one-tenth of the real one. Figure 5.1 gives an idea about the real proportions of a prototype: the visual impact is significantly reduced.

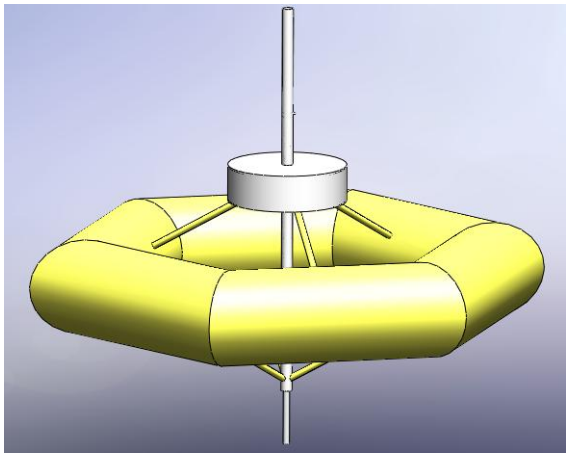

Figure 5.1: How the real buoy can look like.

Chapter 6

Future work

The next step will be to realize a prototype of the model in the full scale. Of course, it will imply more detailed studies about different topics.

The first issue is the storage of power necessary to move the motor. Batteries are the solution, but what batteries, how to connect them to the generator, how long they will last, etc. are problems to be solved.

Moreover, is it possible to avoid the use of lubricant in the prototype? If not, different kinds of lubricants have to be evaluated, in order to choose a non-toxic substance, maybe biodegradable. Once the most suitable lubricant is selected, a safe way to inject it has to be found.

Furthermore, new solutions to prevent the infiltration of water in the housing, where the mechanical components, the motor and the batteries are placed, must be investigated.

Besides, the screw should be moved when the forces on the wire are the smallest, i.e. as the buoy moves from crest to trough and the translator is being dampened by the stator. This will require the development of a system to measure the force on the wire and communicating this to the motor control system.

Finally, a sensor that measures the water level must be placed somewhere, e.g. upon an observation tower placed in the sea or on land. A suggestion can be

to install a wireless system to send information about the current level from the sensor to the motor.

Although a lot of other questions must be answered, these are issues from where to start.

Acknowledgments

I would like to thank Mats Leijon and Giuseppe Passoni not only because they gave me the possibility to develop this thesis, but also because they gave me the opportunity to discover Sweden.

Thanks to Rafael Waters for his kindness and patience, thank you for showing me Lysekil and its real buoys.

Thank you, Markus, for giving me support in every step of my work and for sharing with me your knowledge on this topic.

Thanks to Johan who encouraged me when I could't find the solution and gave me useful tips.

I would also like to thank Juan for his helpfulness and Mattias, Olle, Rickard, Halvar, Magnus, Erland for their advice.

Thanks to Ulf, who helped me in the assembly of my model, and Thomas, for the computer support.

Finally, a big TACK to all the department for warmly welcoming me.

References

[1] A. Skoglund, M. Leijon, A. Rehn, M. Lindahl, R. Waters. On the physics of power, energy and economics of renewable electric energy sources - Part II; August 2009.

[2] M. Leijon. Foreseeable cost reductions in energy from renewables. Stockholm, Sweden, 2004. Proc. of Euroscience Open Forum, invited lecture.

[3] J. Brooke. Wave energy conversion, volume 6, Elsevier ocean engineering book series. Elsevier, Oxford,UK, 2003.

[4] Pelamis Wave Power, http://www.pelamiswave.com/, February 2011.

[5] Wave Dragon, http://www.wavedragon.net/, February 2011.

[6] The Queen's University of Belfast. Islay Limpet Wave Power Plant. Publishable report 1 November 1998 to 30 April 2002. Research founded in part by THE EUROPEAN COMMISSION in the framework of Non Nuclear Energy Programme JOULE III.

[7] R.Waters, J. Engström, J. Isberg, and M. Leijon. Wave climate off the Swedish west coast. Renewable Energy, 2009.

[8] R.Waters, Energy from Ocean Waves - Full Scale Experimental Verification of a Wave Energy Converter. PhD thesis, Uppsala University, Division of Electricity, 2008.

[9] O. Langhamer and D Wilhelmsson. Wave power devices as artificial reefs. Porto, Portugal, 2007. Proc. of the 7th European Wave and Tidal Energy Conference.

[10] J. Sundberg and O. Langhamer. Environmental questions related to pointabsorbing linear wave-generators: impacts, effects and fouling. Glasgow, Scotland, 2005. Proc. of the 6th European Wave and Tidal Energy Conference.

[11] T.W. Thorpe and M.J. Picken. Wave energy devices and the marine environment. IEE Proceedings A (Science, Measurement and Technology), 140(1):63 - 70, 1993.

[12] Swedish Environmental Protection Agency, http://www.naturvardsverket.se/en/In-English/Start/Environmental-objectives/Swedens-environmental-objectives/National-agencies-responsible/, February 2011.

[13] Division for Electricity, Uppsala University. Wave Power Project - Lysekil, http://www.el.angstrom.uu.se/forskningsprojekt/WavePower/Lysekilsprojektet-E.html, April 2011.

[14] Highest tides in the world, http://bayoffundy.com/about/highest-tides/, January 2011.

[15] Tides around the world, http://www.aviso.oceanobs.com/en/applications/ocean/tides/tides-around-the-world/index.html, February 2011.

[16] D.Hareide et al., Water level observations from southwestern coast of Norway. Norwegian Mapping Authority, 2005.

[17] Virginia Institute of Marine Science, http://web.vims.edu/physical/research/ TCTutorial/longwaves.htm, February 2011.

[18] National Instruments. LabVIEW, User Manual. April 2003. Part Number 320999E-01.

[19] J.Fryk,

[20] National Instruments, http://sine.ni.com/np/app/main/p/ap/motion/lang/en/pg/1/sn/n17:motion/fmid/112, December 2010.

[21] Istituto Pesenti, http://www.istitutopesenti.it/dipartimenti/meccanica/Meccanica/ATTRITO.pdf, January 2011.